Capture of mouse and human stem cells with features of formative pluripotency

Masaki Kinoshita[1,5], Michael Barber[1,6], William Mansfield[1], Yingzhi Cui[2], Daniel Spindlow[1,4], Giuliano Giuseppe Stirparo[1,4], Sabine Dietmann[1,7], Jennifer Nichols[1,3] and Austin Smith[1,2,4,5*]

[1] Wellcome-MRC Cambridge Stem Cell Institute
Jeffrey Cheah Biomedical Centre
University of Cambridge
Cambridge CB2 0AW
United Kingdom
[2] Department of Biochemistry
University of Cambridge
Cambridge CB2 1GA
United Kingdom
[3] Department of Physiology, Development and Neuroscience
University of Cambridge
Cambridge CB2 3DY
United Kingdom
[4] Living Systems Institute
University of Exeter
Exeter EX4 4QD
United Kingdom

[5] Authors for correspondence: mk704@cam.ac.uk; austin.smith@exeter.ac.uk

*Lead contact: austin.smith@exeter.ac.uk

Current addresses:
[6] MRC Human Genetics Unit, University of Edinburgh, Edinburgh, EH4 2XU, Scotland, United Kingdom
[7] Department of Developmental Biology and Division of Nephrology, Washington University School of Medicine, St Louis, MO, USA

SUMMARY

Pluripotent cells emerge as a naïve founder population in the blastocyst, acquire capacity for germline and soma formation, and then undergo lineage priming. Mouse embryonic stem (ES) cells and epiblast stem cells (EpiSCs) respectively represent the initial naïve and final primed phases of pluripotency. Here we investigated the intermediate formative stage. Using minimal exposure to specification cues, we derived stem cells from formative mouse epiblast. Unlike ES cells or EpiSCs, formative stem (FS) cells responded directly to germ cell induction. They colonised somatic tissues and germline in chimaeras. Whole transcriptome analyses showed similarity to pre-gastrulation formative epiblast. Signal responsiveness and chromatin accessibility features reflect lineage capacitation. Furthermore, FS cells showed distinct transcription factor dependencies, relying critically on Otx2. Finally, FS cell culture conditions applied to human naïve cells or embryos supported expansion of similar stem cells, consistent with a conserved staging post on the trajectory of mammalian pluripotency.

INTRODUCTION

Mouse embryonic stem (ES) cells correspond to naïve epiblast, a transient population in the pre-implantation embryo (Hackett and Surani, 2014; Smith, 2017). As the embryo implants, naïve pluripotency transcription factors are down-regulated and ability to form ES cells is lost, while transcription factors such as Otx2 and Pou3f1 are up-regulated together with *de novo* methyltransferases Dnmt3a and Dnmt3b (Acampora et al., 2016; Auclair et al., 2014; Boroviak et al., 2014; Boroviak et al., 2015; Brook and Gardner, 1997). After this transition epiblast cells manifest competence for primordial germ cell induction (Ohinata et al., 2009). Subsequently the epiblast becomes progressively regionally fated and molecularly diverse (Beddington and Robertson, 1998; Cheng et al., 2019; Lawson et al., 1991; Peng et al., 2016; Peng et al., 2019). These events are mirrored by ES cells entering into differentiation (Hayashi et al., 2011; Kalkan et al., 2017; Mulas et al., 2017). We hypothesise that exit from naïve pluripotency heralds a formative conversion that instates competence for both soma and germline induction (Kalkan and Smith, 2014; Kinoshita and Smith, 2018; Smith, 2017).

Cultures termed epiblast-derived stem cells (EpiSC) have been obtained by exposure of embryo explants to fibroblast growth factor (FGF) and activin (Brons et al., 2007; Guo et al., 2009; Tesar et al., 2007). EpiSCs can be derived from all stages of epiblast (Kojima et al., 2014; Najm et al., 2011; Osorno et al., 2012), but invariably converge on mid-gastrula stage phenotypes, generally displaying transcriptome relatedness to primed epiblast of the anterior primitive streak (Kojima et al., 2014; Tsakiridis et al., 2014). Thus, culture of epiblast in relatively high levels of FGF (12.5ng/ml) and activin (20ng/ml) results in propagation of a form of primed pluripotency, which is likely dictated by these strong growth factor signals.

Notably, EpiSCs are refractory to primordial germ cell induction, unlike E5.5-6.5 epiblast. (Hayashi et al., 2011; Murakami et al., 2016; Ohinata et al., 2009). Naive ES cells are also unresponsive to germ cell inductive stimuli, unless they are transitioned for 24-48hrs into a population termed epiblast-like cells (EpiLCs) (Hayashi et al., 2011; Nakaki et al., 2013). EpiLCs are molecularly as well as functionally distinct from both naïve ESCs and EpiSCs (Buecker et al., 2014; Hayashi et al., 2011; Kalkan et al., 2017; Smith, 2017). They are enriched in formative phase cells related to pre-streak epiblast, but are heterogeneous and persist only transiently (Hayashi et al., 2011).

Here we invested in an effort to capture and propagate stem cells representative of mouse post-implantation epiblast between E5.5-E6.0, when the formative transition is expected to be completed but epiblast cells remain mostly unspecified.

RESULTS

Derivation of stem cell cultures from mouse formative epiblast

We hypothesised that shielding formative epiblast cells from lineage inductive stimuli while maintaining autocrine growth and survival signals may stall developmental progression but sustain propagation. Nodal, FGF4 and FGF5 are broadly expressed in the early post-implantation epiblast (Haub and Goldfarb, 1991; Mesnard et al., 2006; Niswander and Martin, 1992; Varlet et al., 1997) and promote lineage capacitation in mouse ES cells (Hayashi et al., 2011; Kunath et al., 2007; Mulas et al., 2017; Stavridis et al., 2007). They are therefore

candidates for supporting formative pluripotency. However, together with Wnt3 and bone morphogenetic proteins (BMPs), these growth factors also drive specification in the gastrula (Liu et al., 1999; Winnier et al., 1995).

We speculated that in a context of Wnt inhibition and absence of BMP, moderate stimulation of FGF and Nodal pathways may sustain a formative population. We used the Tankyrase inhibitor XAV939 to block canonical Wnt signalling and excluded undefined components such as feeders, serum, KSR or matrigel. Autocrine Nodal is known to be down-regulated *in vitro* in the absence of extraembryonic tissues (Guzman-Ayala et al., 2004), therefore we added activin A (20ng/ml) as a substitute. E5.5 epiblasts were isolated by microdissection and plated intact in individual fibronectin-coated 4-well plates in N2B27 medium under 5% O_2 (Figure 1A). After 5-6 days, explants were treated with accutase for 5-10 seconds then gently detached, fragmented into small clumps, and seeded into fresh 4-well plates. With or without added FGF, colonies of tightly packed epithelioid cells grew up that could be passaged further and expanded into continuous cell lines (Figure 1A and S1A). In the absence of FGF we observed appreciably higher expression of primitive streak markers Brachyury, FoxA2, Eomes and Gsc, (Figure S1B, C). Nodal/activin signalling is known to stimulate these genes (Brennan et al., 2001; Conlon et al., 1994; Takenaga et al., 2007). We titrated activin and found that continuous cultures could still be established in the absence of FGF (Figure 1B and S1D). In low activin (3ng/ml) plus XAV939 ($A_{lo}X$) we obtained cell lines that could be propagated for more than 20 passages (Figure 1B, S1D, Supplemental movie 1).

Cell lines derived in $A_{lo}X$ expressed *Otx2*, consistent with post-implantation identity, but showed no expression of *T* and minimal *FoxA2* (Figure 1C, D). They displayed similar levels of *Pou5f1 (Oct4)* mRNA to EpiSCs, slightly higher *Sox2*, and lower *Nanog*. (Figure 1C). Upon embryoid body formation and outgrowth, we detected germ layer markers indicating multi-lineage differentiation (Figure 1E).

These observations suggest that in the absence of other stimuli, limited stimulation of the Nodal/activin pathway combined with autocrine FGF activity may suspend cells in the formative phase of pluripotency.

Stem cell propagation is facilitated by retinoic acid receptor inhibition and requires Nodal pathway activity

During establishment and expansion in $A_{lo}X$ we observed sporadic expression of neural lineage markers and appearance of neuronal morphologies. On occasion differentiation was extensive and led to loss of cultures. We speculated that retinoids might be acting as neural inductive stimuli (Bain et al., 1995; Stavridis et al., 2010). We therefore applied a pan-retinoic acid receptor inverse agonist (RARi, BMS 493; 1.0μM) (Figure S1E). Supplementation of $A_{lo}X$ with RARi, henceforth $A_{lo}XR$, resulted in improved derivation efficiency (Figure S1F), reduced ectopic expression of neural specification factors Sox1 and Pax6 (Figure S1E), and stabilised long-term cultures. Using $A_{lo}XR$ we established nine cell lines from embryos of two different strains, 129 and CD1. These lines were all passaged more than 10 times (30 generations) with no indication of crisis or senescence. Established cultures expanded slightly slower than EpiSCs and similar to ES cells, with routine passaging every 2-3 days at a split ratio of 1/10-1/15. Chromosome counts showed a majority of diploid cells even at later passages (Figure S1G). Cells were routinely passaged by mild dissociation into small clumps. Survival was

poor after dissociation to single cells but addition of Rho kinase inhibitor (ROCKi) (Watanabe et al., 2007) enabled reliable clonal expansion.

Using fluorescent *in situ* hybridisation we detected a prominent cloud of Xist expression in nuclei of a female line (Figure S1H). Up-regulation of Xist is indicative of initiation of X chromosome inactivation, a predicted feature of formative epiblast (Mak et al., 2004; Shiura and Abe, 2019).

Mouse ES cells undergo formative transition when withdrawn from 2iLIF (Hayashi et al., 2011; Kalkan et al., 2017; Mulas et al., 2017). We applied A_{lo}XR during this transition and obtained continuously proliferating epithelial cells. Cultures displayed variable levels of heterogeneity during the first few passages (Figure S1I) but stabilised within 4-6 passages and subsequently expanded similarly to embryo derived FS cells. We replated cultures in 2iLIF, which supports clonal propagation of ES cells at high efficiency (Kalkan et al., 2017). All cells died or differentiated within a few days, demonstrating complete extinction of ES cell identity. This finding is in marked contrast to other reports of "intermediate" pluripotent states, which readily revert to ES cells (D'Aniello et al., 2016; Neagu et al., 2020; Rathjen et al., 1999).

Germline and somatic lineage induction in vitro

In mouse, the formative phase of pluripotency is definitively distinguished from naïve and primed phases by competence for germline specification (Hayashi et al., 2011; Ohinata et al., 2009). We examined the response of embryo-derived A_{lo}XR cells to the cytokine cocktail for primordial germ cell (PGC) induction (Ohinata et al., 2009). In each of 8 independent lines tested we detected the PGC surface marker phenotype $CD61^{+}SSEA1^{+}$ (Figure 1F). This capacity was maintained even in late passage (>P30) cultures. The proportion of marker positive cells ranged up to >30% in some experiments, and was generally between 5-25%, although one line was consistently less efficient, around 1%. Two lines expanded without RARi also produced $CD61^{+}SSEA1^{+}$ immunopositive cells, albeit at <10% (Figure S1J). In contrast, 4 AFX EpiSC lines derived from E5.5 epiblast did not yield double positive cells (Figure S1K). Furthermore, AFX EpiSCs adapted to culture in A_{lo}XR over several passages remained unable to produce primordial germ cell-like cells (PGCLC) (Figure S1L).

To confirm PGCLC identity, we sorted the $CD61^{+}SSEA1^{+}$ population and verified expression of a range of germ cell markers by RT-qPCR (Figure S1M). We also observed co-expression of Oct4, Blimp1 and Stella proteins by immunostaining in both A_{lo}XR and A_{lo}X cultures (Figure 1G, S1N). Collectively these features constitute recognised hallmarks of mouse PGCLC (Hayashi et al., 2011; Ohinata et al., 2005). Based on this competence we designated A_{lo}X and A_{lo}XR cells as formative stem (FS) cells.

We then investigated directed somatic differentiation of FS cells in comparison with EpiSCs. Inhibition of the Wnt pathway shifts the character of EpiSCs towards anterior epiblast identity and predisposes them to neuroectodermal fate (Osteil et al., 2019; Tsakiridis et al., 2014). We used the Sox1::GFP reporter (Stavridis and Smith, 2003) to quantify neural induction kinetics of FS cells and EpiSCs maintained with Wnt inhibition. After transfer into permissive N2B27 medium, more than 80% of EpiSCs became GFP positive on day 1 compared with only around 25% of FS cells (Figure 2A). By day 2, however, the GFP+ fraction approached 80% for FS cells and by day 3 reached >80% as for EpiSCs. We examined protein expression by immunostaining and found that FS cells lagged behind EpiSCs in both down-regulation of Oct4

and up-regulation of Sox1, but by day 3 the vast majority were Oct4-negative and Sox1-positive (Figure 2B). Thus, mouse FS cells have similar capacity to form neuroectoderm as EpiSCs but take longer to do so.

We tested primitive streak-like induction in response to activin and GSK3 inhibition (Burgold et al., 2019). We observed substantially higher induction of mesendoderm surface markers and gene expression from FS cells than from EpiSCs (Figure S2A-C). Using flow cytometry we quantified $Flk1^{+}Ecad^{-}$ lateral mesoderm and $Cxcr4^{+}Ecad^{+}$ definitive endoderm. We detected no induction of either lineage directly from ground state ES cells and only modest induction from EpiSCs (Figure 2C and 2E). Across a panel of FS and EpiSC lines induction of mesoderm was on average three-fold more efficient from FS cells (Figure 2D), and of endoderm four-fold higher (Figure 2F).

To probe the basis of differential propensity for primitive streak induction we examined the response of ESCs, FS cells and EpiSCs to signals operative during gastrulation. Ground state ESCs did not up-regulate *T* in response to any stimulus tested with the exception of very low induction by the GSK3 inhibitor CH. EpiSCs also failed to show any appreciable response, apart from induction by CH at 6hrs that was not maintained at 24hrs. In contrast, FS cells showed sustained up-regulation of *T* upon treatment with activin, FGF, CH, or, to a lesser extent, BMP (Figure 2G). Notably, addition of FGF at only 1ng/ml induced *T* and *FoxA2* expression in FS cells (Figure S2D)

Thus, FS cells show rapid and efficient responsiveness to primitive streak inductive cues but require 48 hours for full neural specification. These behaviours are distinct from EpiSCs, and consistent with a developmental stage of E5.5-6.0 epiblast.

Chimaera colonisation

EpiSCs (AF) do not normally contribute to blastocyst injection chimaeras unless they have been genetically modified to enhance ICM integration or survival (Masaki et al., 2016; Ohtsuka et al., 2012; Tesar et al., 2007). We confirmed this finding for AFX EpiSCs derived from E5.5 epiblast, detecting no mid-gestation chimaeras after blastocyst injection of three lines and transfer of 95 embryos. We tested whether FS cells may have higher probability of enduring from the E3.5 blastocyst until stage-matched early post-implantation epiblast. Following blastocyst injection of three different embryo-derived FS cell lines engineered to express mKO2 or GFP we saw reporter expression in multiple E9.5 embryos (Figures 3A, S3A-E). Contributions are low to moderate compared with typical ESC chimaeras and tend to be patchy rather than evenly dispersed. Nonetheless, colonisation may be spread over multiple tissue types, including Sox2 positive putative migratory primordial germ cells (Figure 3B). We examined genital ridge contribution at E12.5 and detected mKO2 reporter positive $Oct4^{+}$ Mvh^{+} primordial germ cells (Figures 3C, S3F, G). By fluorescence imaging we observed contributions to three newborn pups. Two of these animals developed to adulthood and one was euthanised at P21 due to malocclusion. Post-mortem tissue inspection revealed contributions to brain, bone, skin, heart, lung and gut (Figure 3D). In addition, we obtained one overt coat colour chimaera (Figure 3E).

Chimaera formation conceivably might entail reversion of FS cells to naïve status in the blastocyst. We therefore inspected embryos 24 hours after injection. FS cells were localised to the ICM, but immunostaining showed that in contrast to host naïve epiblast or introduced

ES cells, FS cells did not express the naïve pluripotency specific transcription factor Klf4 and retained the formative marker Oct6 (Figure 3E). Therefore, FS cells maintain formative identity within the blastocyst environment.

Chimaera formation by FS cells derived from post-implantation epiblast challenges the conclusion from classic embryo-embryo chimaera studies that epiblast cells lose colonisation ability entirely by E5.5 (Gardner and Brook, 1997; Gardner et al., 1985). We revisited those experiments using a fluorescent reporter to allow sensitive detection of contributions. We dissected epiblasts from cavitated E5.5 and pre-streak E6.0-6.25 transgenic embryos expressing membrane-bound tdTomato (mTmG). Epiblasts were dissociated using Accutase with addition of ROCKi to improve viability and 10 cells injected per blastocyst. We detected tdTomato positive cells in 11 out of 91 embryos recovered at E9.5 (Figures 3F, G, S3H-S3L). Contributions were typically sparse and interestingly were most frequent in yolk sac mesoderm and amnion. In three chimaeras, however, colonization was widespread in the embryo proper (Figures 3F, G, S3H). We did not detect any contribution from streak stage (E6.5-7.0) epiblast cells (Figure S3L).

These observations establish that FS cells and primary formative epiblast cells can contribute to blastocyst chimaeras, although with lower efficiency than ES or ICM cells.

Transcriptome relatedness to pre-streak epiblast

For global evaluation of cellular identity we performed RNA-seq. We first compared FS cells with ground state ES cells and with EpiSCs cultured in AF or AFX. Principal component analysis (PCA) grouped ES cells apart on PC1 while the two types of EpiSCs and FS cells were resolved on PC2 (Figure 4A). Differential expression analysis (Log_2 fold change > 1.4, adjusted P value < 0.05) identified 531 and 266 genes up-regulated and 941 and 168 genes down-regulated in FS cells relative to AF and AFX EpiSCs respectively (Figure S4A ad S4B). GO term enrichment analysis highlighted “cell adhesion” in FS cells, contrasting with gastrulation and development in EpiSCs (Figures S4A,B). We identified 328 genes that are up-regulated in FS cells compared with ES cells or either class of EpiSC (Figure 4B), with GO term enrichment for “ion transport” and “cell adhesion” (Figure 4C).

We then used a low cell number RNA-seq protocol with deep read depth (Boroviak et al., 2015) for comparison of FS cells with dissected pre-cavitation (E5.0), early cavitation (E5.5), and pre-streak (E6.0) epiblast. Unsupervised hierarchical clustering showed FS cell relatedness to E5.5 and E6.0 epiblast, with lower correlation to the pre-cavitation stage (Figure 4D). EpiSCs, both AF and AFX, were less related to the pre-gastrula epiblast stages. We identified 953 differentially expressed genes between FS cells and EpiSCs. This gene set clustered published embryo and EpiLC single cell data (Nakamura et al., 2016) by developmental trajectory (Figure 4E). Our RNAseq E5.5 and E6.0 epiblast profiles projected onto this PCA aligned with E5.5 and EpiLC single cells (Figure 4E). FS cells overlapped with EpiLCs, between E5.5 and E6.5 T_{Lo}, whereas EpiSCs were positioned with the E6.5 cells. We inspected several of the FS cell specific genes (Figure 4B) and detected dynamic expression in the embryo single cell data with enrichment at E5.5 (Figures 4F, S4C).

We performed single cell analysis on FS cells and EpiSCs using the Smart2-seq method (Picelli et al., 2014). Applying a threshold of 3M reads we examined 326 cells. FS cells from two independent lines formed a single cluster in the PCA plot (Figure 4G), separated from

EpiSCs on PC1. Notably there was no overlap between EpiSCs and FS cells. PC2 separated AF and AFX EpiSCs. Measurement of gene expression correlation by Jaccard index showed that FS cells are more homogeneous than either class of EpiSC (Figure 4H).

Collectively these analyses indicate that FS cells capture features of pre-streak epiblast and EpiLCs, but are less related to later stage epiblast and EpiSCs.

Growth factor requirements for FS cell propagation

As potential autocrine stimuli of self-renewal or differentiation, we evaluated Nodal, FGF and Wnt family representation in the FS cell transcriptome data (Figures S4D-F). We found robust expression of *Fgf5* as expected but also detected several other FGFs at lower levels. However, *Fgf8* which is active during primitive streak formation (Sun et al., 1999), was lowly expressed compared with EpiSCs. FS cells express both *Fgfr1* and *Fgfr2* (Figure S4D). We tested whether FS cell cultures are dependent on FGF signalling by adding specific inhibitors of FGF receptors (PD173074, 0.1μM) or downstream MEK1/2 (PD0325901,1μM). Both inhibitors caused rapid collapse of FS cell cultures. We conclude that endogenous low-level expression of FGFs supports self-renewal, without inducing the primitive streak-associated gene expression associated with exposure to exogenous FGF (Figures 2G, S2D).

FS cells express nodal/activin receptors but interestingly present lower mRNA levels for the co-receptor *Tdgf1* and for *Nodal* itself than either ES cells or EpiSCs (Figure S4E). We investigated further the requirement for nodal pathway stimulation. Addition of receptor inhibitors (A83-01 or SB505124) resulted in extensive cell death and differentiation with loss of Oct4 and up-regulation of Pax6 (Figures 4I,S4G). Withdrawal of activin also led to reduced viability and increased differentiation, indicating that autocrine activity does not provide sufficient pathway stimulation. In FS cell medium activin is added at only 3ng/ml compared with 20ng/ml typically used for feeder-free culture of EpiSCs. Dosage sensitivity is a well-known feature of nodal signalling in the mouse embryo (Robertson, 2014). We observed markedly less induction of nodal pathway targets in FS cells at 3ng/ml compared to 20ng/ml activin (Figure 4J). Furthermore, immunoblotting indicated lower steady state levels of phospho-Smad2 in cells passaged in 3ng/ml activin (Figure 4K). These observations are consistent with a dose-dependent response to nodal/activin stimulation, whereby low signal sustains the formative gene regulatory network and higher signal promotes primitive streak specification.

Finally, the observed expression of Fzd receptors and low levels of some Wnts may underlie the requirement for inhibition of Wnt signalling to fully suppress differentiation (Figure S4F). Consistent with this interpretation we observed that the porcupine inhibitor IWP2 could substitute for XAV939 during FS cell maintenance.

Thus, FS cells are maintained by FGF and nodal/activin but are poised to respond to increased levels of either signal or of canonical Wnt by entering into mesendoderm differentiation.

Chromatin accessibility in formative stem cells

We employed the assay for transposase accessible chromatin coupled to deep sequencing (ATAC-seq) (Buenrostro et al., 2013) to survey open chromatin in FS cells. Independent FS cell samples were well correlated (Figure 5A). We classified sites that exhibit differential

accessibility between ES, FS and EpiSCs based on a fold-change enrichment greater than two (p-value<0.05). Reorganisation was evident between naïve and formative cells, with 3742 sites closing, 4259 opening and only 207 shared open sites (Figures 5B,C). In contrast, between formative and primed cells, a majority of open sites were shared (3588), while just over 1000 became more accessible and a similar number closed. We detected 826 peaks specifically enriched in FS cells compared to either ES cells or EpiSCs. These FS cell-specific open chromatin regions were also accessible in transient EpiLCs (Figures 5C,D). Nearby genes (<1kb) showed no significant GO term enrichment, however (Figure S5A).

ChIP-seq for histone modifications showed the expected correlation between open chromatin and active marks, H3K4me3, H3K4me1 and H3K27Ac (Fig.5E). Regions that were more open in naïve and formative cells showed marked enrichment for H3K4me3 and H3K27ac that was lost in EpiSCs. Interestingly, active marks were also more highly represented in FS cells than in ES cells at loci that opened only in EpiSCs. We surveyed bivalent promoter regions marked with both H3K4me3 and H3K27me3 (Azuara et al., 2006; Bernstein et al., 2006). We enumerated 2417 bivalent promoters in FS cells, nearly three times the number in ES cells (Figure S5B). Many, but not all, of these loci were also bivalent in EpiSCs. Figure S5C shows examples of different profiles. Among the FS cell specific bivalent promoters was *Prdm14*, encoding one of the key germ cell determination factors (Nakaki et al., 2013). Promoters for other germ cell genes *Tfap2c* and *Prdm1* are also bivalent in FS cells, consistent with being poised for expression (Figure 5F). In EpiSCs, however, *Prdm14* loses both marks indicating the gene is inactivated. This chromatin change may be a decisive feature in the loss of competence for PGCLC induction in EpiSCs (Hayashi et al., 2011)

We also assessed DNA methylation at open chromatin regions using published data for EpiLCs and EpiSCs (Zylicz et al., 2015). In EpiLCs all ATAC peaks were hypomethylated. In EpiSCs, in contrast, only primed peaks maintained low methylation (Figure S5D).

Among genes proximal to shared ATAC peaks in FS cells and EpiSCs, we observed marked differential expression (Figure 5G). GO term analysis of genes more highly expressed in EpiSCs identified enrichment for heart development, multicellular organism development and gastrulation (Figure S5E). These included gastrulation-associated genes such as *Cer1*, *Gsc*, and *Pax3*. FS cell enriched transcripts were more numerous but comprised genes without annotated functions in early development (Table S1).

We used HOMER (Heinz et al., 2010) to identify transcription factor binding motifs enriched in open chromatin regions (Table S2). Core pluripotency factor binding motifs for Oct4 and Oct4-Sox-Tcf-Nanog were over-represented in all three cell types. ES cell ATAC peaks were also enriched for Tfcp2l1 and Prdm14 motifs, while those in EpiSCs featured Gsc, Brachyury, Slug, and Eomes motifs (Figures 5H,S5F). Both FS cells and EpiSCs showed increased accessibility of AP1/Jun sites. Finally, we noted that FS cell open chromatin showed specific enrichment for ETS-domain factor binding motifs.

FS cells and EpiSCs show contrasting dependencies on Etv and Otx2

Previously we presented evidence linking Etv5, an ETS factor of the PEA3 sub-family, to enhancer activation during pluripotency progression (Kalkan et al., 2019). We also showed that ES cells lacking Etv5 show diminished ability to make EpiSCs. Here we employed CRISPR/Cas9 to generate ES cells deficient for both *Etv5* and the related *Etv4*. *Etv4/5*-dKO cells failed completely to produce EpiSCs upon transfer to AFX and differentiated into

fibroblast-like cells (Figure S6A). This phenotype is more severe than for *Etv5* mutation alone. Somewhat unexpectedly, however, *Etv4/5*-dKO cells converted to epithelial culture in A_{lo}XR and subsequently expanded, albeit with persisting differentiation (Figures 6A, S6A). Relative to ESCs, naïve factors were down-regulated and post-implantation markers up-regulated, including several targets of Etv5 such as *Fgf5*, *Otx2* and *Pou3f1* (Figure 6B). We detected no compensatory up-regulation of the third PEA3 member, *Etv1*. *Etv4/5*-dKO FS cells differentiated readily via embryoid bodies and in directed protocols (Figure S6B-E), including induction of Blimp1$^+$, Stella$^+$, Oct4$^+$ PGCLC (Figure S6F). However, when transferred to AFX, *Etv4/5*-dKO cells failed to convert to EpiSCs, lost expression of Oct4 within 3 days, and differentiated into fibroblasts with aberrant expression of *Pou3f1* (Figures 6C,D,S6G). Introduction of an *Etv5* transgene to *Etv4/5*-dKO cells restored the ability to convert to EpiSCs (Figure 6E-H). These results establish that Etv4 and Etv5 are not essential for lineage competence of FS cells yet are required for production of EpiSCs *in vitro*.

Otx2 is prominently up-regulated early during formative transition in vivo and in vitro (Acampora et al., 2016; Kalkan et al., 2017), and is implicated in redirecting genome occupancy of Oct4 (Buecker et al., 2014; Yang et al., 2014). Intriguingly, *Otx2* is dispensable in both ES cells and EpiSCs (Acampora et al., 2013), but homozygous embryo mutants exhibit severe gastrulation phenotypes (Ang et al., 1996). We generated *Otx2* KO ES cells and investigated conversion into FS cells in A_{lo}XR. Epithelial colonies emerged and could be expanded for 4-5 passages but continuously differentiated into neural cells (Figure 6I). By passage 5 Oct4 and Nanog were downregulated and the majority of cells were positive for Sox1 (Figure 6J). Cultures could not be maintained reliably thereafter. In contrast *Otx2* mutant ES cells could be converted into stable Oct4 positive EpiSCs by direct transfer into AFX (Figure 6I), although colonies frequently displayed aberrant expression of Sox1 as previously reported (Acampora et al., 2013)(Figure 6J). BMP has been shown to enhance stability of *Otx2* deficient EpiSCs (Acampora et al., 2013). We added BMP to two *Otx2*$^{-/-}$ FS cell cultures in A_{lo}XR but observed no suppression of differentiation (Figure S6H).

We also mutated *Otx2* directly in FS cells and observed that colonies became compact and dome-shaped, superficially resembling naive ES cells (Figure 6K,L,M). When replated in 2iL, however, *Otx2* mutant FS cells did not expand but differentiated or died (Figure S6I). We managed to achieve initial clonal expansion of targeted FS cells in A_{lo}XR, but 8 out of 8 clones subsequently underwent extensive neural differentiation and could not be stably propagated. We added BMP to three cultures, but this did not result in stabilisation.

These results indicate that Otx2 but not Etv4/5 is required for a stable FS cell state, and conversely for EpiSCs.

Generation of human FS-like cells

We explored derivation of FS cells from naïve human pluripotent stem cells (hPSCs) (Takashima et al., 2014). We used both chemically reset lines, cR-H9EOS and cR-Shef6 (Guo et al., 2017), and embryo-derived HNES cells (Guo et al., 2016). A_{lo}X and A_{lo}XR were applied as for mouse FS cell culture, except that plates were coated with a combination of laminin and fibronectin to improve attachment. The domed naïve hPSCs converted to a more flattened epithelioid morphology over several days. Cultures could be propagated continuously thereafter and exhibited a faster doubling rate than naïve cells, requiring passage every 4 days at a split ratio of 1/15 (Figure 7A). Cells in A_{lo}XR lost naïve markers (KLF4, KLF17, TFCP2L1)

but retained the core pluripotency factor OCT4, with little or no up-regulation of lineage priming markers, TBXT or FOXA2, often detected in conventional hPSCs (Figure 7B) (Allison et al., 2018; Gokhale et al., 2015). They showed gain of SOX11 and OTX2, markers of post-implantation epiblast in the primate embryo (Nakamura et al., 2016).

Naïve hPSCs do not respond productively to somatic lineage induction protocols but must first undergo formative transition to lineage competence (Guo et al., 2017). This capacitation process takes place over several days (Rostovskaya et al., 2019). FS cells in contrast are expected to be directly responsive to lineage cues. We applied established protocols for differentiation to human FS cells. In response to definitive endoderm induction (Loh et al., 2014), we observed efficient formation of SOX17 positive cells (Figure 7C), while neural induction via dual SMAD inhibition (Chambers et al., 2009) resulted in abundant SOX1 immunopositive cells (Figure 7D). We also tested paraxial mesoderm differentiation (Chal et al., 2016) and detected up-regulation of *TBX6* and *MSGN1* along with EMT markers such as *SNAIL1* and *ZEB1* (Figure 7E).

We prepared RNA-seq libraries from three human FS-like cell lines and carried out whole transcriptome comparison with naïve and conventional hPSCs (Figure 7F). PCA distinguished naive cells on PC1 and separated formative from conventional hPSCs on PC2, similar to the analysis of mouse PSCs (Figure 4A). As a reference for in vivo early post-implantation development we used data for the non-human primate *Macaca fascicularis* (Nakamura et al., 2016). We computed the PCA for *Macaca* using 9324 expressed orthologous genes (median Log2 expression>0.5) onto which we projected the human cell line samples (Figure 7G). FS-like cells and conventional hPSCs aligned with post-implantation embryo stages. FS-like cell samples were positioned with post-implantation epiblast while conventional hPSCs spread further towards early gastrulating cells.

Single cell transcriptome data has recently been published for human embryos during extended culture (Xiang et al., 2019). We used variable genes in the epiblast and primitive streak anlage (PSA) stages to compute the PCA for naïve, formative and conventional hPSCs and then projected the embryo single cells. The resulting plot shows a similar pattern to the *Macaca* embryo comparison. Naïve cells clustered with pre-implantation epiblast and formative cells were next to post-implantation stages. Conventional hPSCs were adjacent to FS cells but distributed more towards the PSA cluster (Figure 7H).

We performed K-means clustering (k=6) between FS-like and conventional PSC cultures (Figure S7A). Cluster 1 comprises 369 genes expressed more highly in FS cells than conventional hPSCs. The majority of protein-coding genes in this cluster are expressed in naïve cells and persist during capacitation (Figure S7B, C). *DPPA2*, *GDF3* and several *ZNF* genes were identified as useful markers expressed in both naïve and formative cells but variably low or absent in conventional hPSCs (Figure 7I, S7D). Expression of these ZNF genes was detected in human pre- and post-implantation epiblast transcriptome data (Figure 7J).

KRAB-ZNFs such as ZNF676, ZNF560, and ZNF528 can suppress expression of transposable elements (TEs) (Friedli and Trono, 2015). TEs are dynamically expressed in early development and highly differential between naïve and primed hPSCs (Friedli and Trono, 2015; Guo et al., 2017; Theunissen et al., 2016). We examined TE expression in FS-like cells and observed a distinct profile compared with naïve or conventional hPSCs (Figure 7K). For example, FS-like cells distinctively expressed LTR6A, and retained expression of certain

HERVK TEs also expressed in naïve cells, but did not express subsets of SVA family members that are prominent in naive cells, nor subsets of HERVH, LTR7C or LTR12C family members that are prominent in primed cells (Figure S7E).

Finally, we investigated application of FS cell culture conditions directly to human ICM explants which are known to transition to early post-implantation stages (O'Leary et al., 2012). We thawed E5 and E6 blastocysts and cultured for one or two days respectively in N2B27. We then isolated ICMs by immunosurgery or manual dissection and plated them intact on laminin/fibronectin coated dishes in A_{lo}XR with ROCK inhibitor. After 2-4 weeks, primary outgrowths were manually dissociated and re-plated. We established three lines from different embryos. The embryo derived lines exhibited similar morphology and growth behaviour to naïve PSC derived FS-like cells (Figure 7L). G-banded karyotype analysis showed that all three expanded lines were diploid (46XX, 20/20) (Fig.S7F). We confirmed relatively homogeneous expression of OCT4, SOX2 and NANOG by immunostaining (Figure 7M). Expression of naïve-specific transcription factors KLF4 and KLF17 was not detected while transcripts were present for several genes that are expressed in naïve and formative cells but down-regulated in conventional hPSCs (Figure 7N).

DISCUSSION

Expandable stem cells that retain high fidelity to staging posts of pluripotency in the embryo will be instrumental in harnessing capacity to recapitulate development, create disease models, and manufacture therapeutic cells. Stem cells representative of naïve and primed pluripotency have been established in mouse and human (Davidson et al., 2015; Nichols and Smith, 2009; Rossant, 2015; Rossant and Tam, 2017) but formative pluripotency has only been obtained in the form of transient EpiLCs (Buecker et al., 2014; Hayashi et al., 2011; Kalkan et al., 2017; Mulas et al., 2017). The findings in this study fill the stem cell gap between early and late pluripotency.

Mouse ES cell derivatives with features of late blastocyst or peri-implantation epiblast, such as reduced Rex1 or increased Otx2, have been reported previously (D'Aniello et al., 2016; Neagu et al., 2020; Rathjen et al., 1999). However, those cells spontaneously reverted to the canonical ES cell phenotype when transferred to ES cell culture. Therefore, they remain within the naive spectrum. Significantly, the cytokine LIF, which potently promotes mouse ES cell identity (Dunn et al., 2014; Smith et al., 1988; Williams et al., 1988), is a key component of all these culture conditions. In contrast, FS cells are maintained without LIF and have extinguished ES cell identity, in line with the inability of peri-implantation epiblast to form ES cells (Boroviak et al., 2014).

In mouse, a defining functional attribute of formative epiblast is direct responsiveness to germline induction, which is lacking in both naïve cells and primed gastrula stage epiblast (Ohinata et al., 2009). Conversion of ESCs into transient EpiLC populations generates a window of germline competence (Hayashi et al., 2011). However, maintenance of competence over many passages is a unique feature of mouse FS cells, signifying stabilisation of a transient embryonic state.

Mouse FS cells also differ from ES cells and EpiSCs in their contribution to chimaeras. Chimaerism is less frequent, to lower levels, and less evenly distributed than typically obtained with ES cells. Poorer contributions are not unexpected given the heterochronicity between FS cells and E3.5 host blastocysts. Pioneering mouse embryo chimaera studies suggested that blastocyst colonisation capacity was lost entirely after implantation (Gardner, 1985). Here, using more sensitive detection systems and injecting 10 cells rather than single cells with ROCKi to improve viability, we found that formative epiblast cells can contribute to blastocyst chimaeras, similarly to FS cells. EpiSCs in contrast do not generally show any significant contribution to chimaeras via blastocyst injection, unless they have been genetically engineered (Masaki et al., 2016; Ohtsuka et al., 2012; Tesar et al., 2007). Intriguingly, it has been reported that certain EpiSC lines cultured on feeders or serum-coated dishes contain a sub-population of cells that are able to contribute to chimaeras (Han et al., 2010; Kurek et al., 2015). The nature of such cells is unclear, but our results raise the possibility that they may represent FS cells co-existing with EpiSCs in those undefined conditions.

FS cells exhibit distinct signal dependency and responsiveness compared to ESCs or EpiSCs. Both mouse EpiSCs and human conventional PSCs are cultured in medium supplemented with FGF. Indeed, high FGF (100ng/ml) is considered an essential component of defined E8 medium for hPSCs (Chen et al., 2011; Cornacchia et al., 2019). FS cells in contrast are cultured without FGF supplementation. Notably mouse FS cells respond directly to FGF or other stimuli for primitive streak induction by up-regulating *T*. Consistent with readiness for *T* induction, FS cells exhibit greater propensity to form mesendoderm than EpiSCs. We surmise that the relative recalcitrance of EpiSCs to primitive streak induction may reflect adaptation to the high growth factor signals that drive their in vitro proliferation. FS cells are also efficient at entering the neural lineage but, consistent with an earlier stage of epiblast, do so more slowly than EpiSCs. High competence for germline, primitive streak and neural induction are features of pre-streak formative epiblast. Whole transcriptome analysis substantiates this identity and further confirms that mouse FS cells are related to EpiLCs and distinct from EpiSCs.

FS cells and EpiSCs show different transcription factor dependencies. FS cells are mildly destabilised by deletion of *Etv5* and *Etv4* but remain expandable and pluripotent, whereas the EpiSC state cannot be established without these factors (Kalkan et al., 2019). Whether the inability to produce *Etv4/5* dKO EpiSCs results from a cryptic change in formative competence or reflects a specific function in EpiSCs remains to be clarified. Interestingly, a proportion of *Etv5* or *Etv4/5* mutants proceed through gastrulation (Lu et al., 2009; Zhang et al., 2009). The *Etv4/5* knockout phenotypes therefore suggest that the *in vitro* EpiSC state may not be fully representative of epiblast progression *in vivo* (Kojima et al., 2014). Conversely, Otx2, which is necessary for *in vivo* gastrulation (Ang et al., 1996), is not required by ES cells or EpiSCs (Acampora et al., 2013) but is indispensable for stable expansion of FS cells. Defective formative transition may also underlie the increased neural differentiation of EpiSCs lacking Otx2 (Acampora et al., 2013).

In FS cells the transcription factor circuitry governing naïve pluripotency (Dunn et al., 2014; Takashima et al., 2014) is dismantled, signalling pathways rewired, and chromatin accessibility extensively remodelled compared to ES cells. These events indicate a step change as cells transition from naïve to formative pluripotency. By contrast, the separation between FS cells and primed pluripotent stem cells is blurred, in line with more continuous developmental progression. We surmise that the reconfigured gene regulatory network and chromatin landscape in formative cells provide the requisite context for signalling cues to

induce germ layer and germline lineage specification and for the subsequent unfolding of gastrulation. Capture of formative phase cells as self-renewing stem cell cultures should be enabling for comprehensive interrogation of the molecular features that confer and effect multi-lineage potency.

Limitations of Study

Although the formative phenotype is reached within 48hrs of ESC withdrawal from 2i, generation of stable FS cell lines requires several passages. The inherent asynchronicity of exit from naïve pluripotency (Strawbridge et al., 2020) together with imperfect in vitro transition conditions result in initial heterogeneity, as also observed for EpiLC formation (Hayashi et al., 2011; Kalkan et al., 2017). Passaging enriches for FS cells, similar to stabilistaion of EpiSC cultures (Guo et al., 2009), but a more streamlined and efficient capture would be advantageous for future research. In mouse, FS cells are clearly distinguished from EpiSCs by several features, most notably competence for germ cell induction and ability to colonise chimaeras via blastocyst injection. Neither of those functional criteria are applicable in the human context. Conventional hPSCs share some features with EpiSCs but do not appear to be direct equivalents (Lau et al., 2020; Rossant and Tam, 2017). Notably they can be induced to form primordial germ cell-like cells (Irie et al., 2015; Sasaki et al., 2015). Chimaera contribution cannot be tested in human embryos. At the transcriptome level, human FS-like cells differ from populations of conventional hPSCs cultured in E8 or other conditions, but these differences are relative rather than absolute. Heterogeneity and hierarchical substructure has been described in hPSC cultures (Allison et al., 2018; Hough et al., 2009; Hough et al., 2014; Lau et al., 2020; Nakanishi et al., 2019) and we cannot exclude the presence of formative stem cells at some frequency. Human FS cells and conventional hPSCs may be a continuum spanning post-implantation epiblast progression. It will be valuable in future studies to define marker sets and in vitro differentiation behaviours that can better distinguish human formative cells from downstream stages in the spectrum of post-naïve pluripotency. To this end additional transcriptomic and other data on post-implantation epiblast will be important to allow more precise comparison and staging.

Acknowledgements

We thank Vicki Metzis for the ATAC-seq protocol, Elsa Sousa for help with *Xist* FISH, and Meng Amy Li for the gRNA expression vector. Tüzer Kalkan, Nicola Reynolds and Laurence Bates advised on ChIP-seq. We are grateful to Maike Paramor, Vicki Murray, Peter Humphreys, Darran Clements, Andrew Riddell, Charles-Etienne Dumeau and biofacility staff for technical support and to the CSCI core bioinformatics team for data processing and routine analysis. Sequencing was performed by the CRUK Cambridge Institute Genomics Core Facility. Shahzaib Ahmed and Benjamin Porteous contributed to experiments. Rosalind Drummond and James Clarke provided laboratory assistance. We thank Brian Hendrich for comments on the manuscript. The Cambridge Stem Cell Institute receives core funding from Wellcome and the Medical Research Council. This research was funded by the Biotechnology and Biological Sciences Research Council and the Medical Research Council of the United Kingdom. AS is a Medical Research Council Professor.

Author contributions

Conceptualization, AS; methods, MK; formal analysis, MB, DS, GGS, SD; investigation, MK, WM, YC, JN; writing, MK, AS; supervision, AS

Declaration of interests

The authors declare no competing interests

FIGURE LEGENDS

Figure1. Derivation of stem cell lines from formative epiblast.
(A) Schematic of cell line derivation from E5.5 epiblast. (B) Image of serially passaged E5.5 epiblast-derived culture. Scale bar 100µm. (C) RT-qPCR analysis of marker gene expression in $A_{lo}X$ cells and EpiSCs relative to ES cells in 2iL (=1), normalized to beta-actin. Error bars are S.D. from technical triplicates. (D) Immunofluorescent staining of EpiSCs and $A_{lo}X$ cultures for early lineage markers. Scale bars 150µm. (E) Immunostaining of embryoid body outgrowths for germ layer markers, DAPI in blue. Scale bars, 150µm. (F) Flow cytometry analysis of PGCLC induction at day 4. (G) Immunostaining of day 4 PGCLC. Scale bars 50µm.

Figure 2. Lineage potency of FS cells and responsiveness to differentiation cues.
(A) Neural differentiation assayed by quantification of Sox1::GFP-positive cells. Error bars represent S.D. from 4 independent experiments. (B) Immunostaining of FS cells and EpiSCs during neural differentiation, DAPI in white. Scale bars, 100 µm. (C) Lateral plate mesoderm differentiation and representative quantifications of the $Flk1^{+}Ecad^{-}$ fractions by flow cytometry. (D) Average efficiency of Flk1 positive cell production from FS cells and EpiSCs. n = independent cell lines assayed. Error bars represent the S.D. **P<0.01. (E) Definitive endoderm differentiation protocol and representative quantifications of the $Cxcr4^{+}Ecad^{+}$ fraction. (F) Average proportion of $Cxcr4^{+}Ecad^{+}$ double positive cells from differentiation of FS and EpiSC lines. Error bars represent S.D., *P<0.05. (G) *T* expression analysed by RT-qPCR 6h and 24h after transfer into N2B27 medium with the indicated supplements; 2µM XAV939, 20ng/ml activin A, 10ng/ml BMP2, 12.5ng/ml Fgf2 and 3µM CH. Relative expression is normalised to GAPDH. Error bars are S.D. from two independent cell lines and two technical replicates.

Figure 3. Blastocyst chimaera contribution by FS cells and formative epiblast.
(A) Bright field and fluorescent images of E9.5 embryos generated after blastocyst injection of mKO2 reporter FS cells. Scale bar is 1mm. (B) Sagittal section from one chimaera, stained for mKO2 and DAPI. Inset B', mKO2 positive cells in foregut endoderm (yellow arrowheads) and cardiac mesoderm (green arrowheads). Inset B'' (rotated 90^{0}), Sox2 immunostaining (white arrowheads) in the hindgut region. Scale bars, 200µm (B), 100µm (B', B"). (C) mKO2 positive cells expressing Oct4 and Mvh PGC markers in E12.5 chimaeric gonad. Triple positive cells are highlighted with dashed circles. Scare bars, 75µm. (D) Fluorescent images of organs from post-natal (P21) chimaera overlaid with 20% opacity bright field image. Scale bars, 2 mm. (E) Coat colour chimaera at P14. (F) Blastocysts injected with GFP reporter ES cells or FS cells and cultured for 24 hours. ES cells are $Klf4^{+}Oct6^{-}$ (n=11) (F') whereas FS cells are $Klf4^{-}Oct6^{+}$ (F'') (n=15). Scale bars, 40µm. (G) E9.5 chimaeras obtained from blastocyst injection of mTmG expressing E5.5 epiblast cells. Scale bars, 500µm. (H) Section from left embryo in Panel G stained with anti-RFP to visualise membrane-tdTomato, DAPI in blue. Scale bar, 200µm.

Figure 4. Whole transcriptome analysis and nodal/activin pathway activity.
(A) PCA with all genes for ES cells, FS cells and EpiSCs (AFX and AF). (B) Heatmap clustering of naïve, formative and primed enriched genes. (C) GO term analyses based on the genes identified in (B). X-axis is -Log(P-Value). Top 6 significant terms are shown (Benjamini value<0.05). (D) Heatmap comparison of FS cells and AFX and AF EpiSCs with E5.0, E5.5 and E6.0 epiblast cells. (E) Left, PCA with mouse single cell data from embryos and EpiLCs (Nakamura et al 2016). Right, samples from (D) were projected onto the single cell PCA. (F)

Gene expression patterns of selected FS cell enriched genes identified in (B) coloured on PCA from E. E5.5 epiblast cells are highlighted by the dashed circle. (G) PCA using 2000 most abundant genes of scRNA-seq data from two FS cell lines and one AFX and one AF EpiSC line. (H) Violin plot of Jaccard index analysis of 2,000 most abundant genes shows higher correlation between FS cells than EpiSCs. (I) RT-qPCR analysis of FS cells in AloXR (Ctrl) or with addition of 1μM A83-01 or 5 μM SB5124, or withdrawal of activin for 2 days. Relative expression to beta-actin. Error bars are S.D. from technical duplicates. (J) RT-qPCR analysis of FS cells cultured in low (3ng/ml) and high (20ng/ml) activin for two days. Relative expression to beta-actin. Error bars are S.D. from technical duplicates. (K) Western blot analysis of phospho-Smad2 protein. Cells were passaged once with low (3ng/ml) or high (20ng/ml) activin A before collecting protein.

Figure 5. Chromatin landscape analysis.
(A) Hierarchical clustering of all ATAC-seq peaks. (B) Peak changes between states. OC; open to closed, CO; closed to open, OO; open to open. (C) Heatmaps of differential ATAC-seq peaks (D) Heatmaps of ATAC-seq peaks from (C) in EpiLCs and EpiSCs derived from RgD2 ES cells. (E) Histone modification patterns at ATAC-seq peaks. (F) Genome browser screenshots of H3K4me3 and H3K27me3 distribution at *Prdm1*, *Tfap2c* and *Prdm14* loci. (G) Volcano plot showing gene expression fold changes associated with shared ATAC-seq peaks between FS cells and EpiSCs. Purple up-regulated in EpiSCs, blue up-regulated in FS cells. (H) Transcription factor binding motif enrichments at ATAC-seq peaks.

Figure 6. Differential requirements for *Etv4/5* and *Otx2*.
(A) Morphology of *Etv4/5* dKO FS cells. (B) RT-qPCR analysis of ES cells (yellow), parental (WT) FS cells (blue) and *Etv4/5*dKO FS cells (purple). Error bars represents S.D. from technical duplicates. (C) Morphology of WT and dKO FS cells in EpiSC (AFX) culture medium for three days. (D) Time course RT-qPCR analysis of WT and *Etv4/5*dKO FS cells in EpiSC (AFX) culture. Error bars are S.D. from technical duplicates. (E) Morphology of *Etv4/5*dKO FS cells expressing *Etv5* transgene. (F) RT-qPCR assay of *Etv1*, *-4* and *-5* in *Etv5* rescue dKO lines. Error bars represents S.D. from technical duplicates. (G) Morphology of rescued dKO FS cells in EpiSC (AFX) culture. (H) Time course RT-qPCR analysis of rescued lines. Error bar represents S.D. from technical duplicates. (I) Phase images of *Otx2* KO ES cells transferred to FS cell or EpiSC (AFX) culture conditions for 5 passages. (J) Immunostaining of *Otx2* KO cells at p5 in FS cell or EpiSC culture. Two classes of EpiSC colony were observed: left, homogenous Oct4 with heterogenous Nanog and Sox1; right, uniformly Oct4, Sox1 and Nanog triple positive. (K) Alkaline phosphatase (AP) staining of control, *Oct4* and *Otx2* KOs generated by Cas9/gRNA transfection in FS cells and EpiSCs. Colonies were stained three days after replating transfected cells. (L) Morphology of AP positive *Otx2* KO FS cells and EpiSCs. (M) Representative image of *Otx2* KO FS cells before culture collapse. Scale bars 100μm, except (J) 50μm.

Figure 7. Human FS-like cells established from naïve ES cells and embryos.
(A) Morphology of human A_{lo}XR cells derived from naïve hPSCs. Scale bar, 100μm. (B) RT-qPCR expression analysis of marker genes in two human FS cell lines compared with naïve and conventional (primed) hPSCs. Error bars represents S.D. from technical triplicates. (C) SOX17 immunostaining of hFS cells after endoderm induction. (D) SOX1 immunostaining of hFS cells after neural induction. (E) RT-qPCR analysis of hFS cells differentiated into paraxial mesoderm for 6 days. Error bars represent S.D. from technical triplicates. (F) PCA of hFS cells with naïve and conventional hPSCs computed with 11051 genes identified by median Log2

expression >0.5. (G) Projection of human FS cell and conventional PSC samples onto PCA of *Macaca* ICM/epiblast stages computed with 9432 orthologous expressed genes. (H) PCA for cell line populations computed using 922 variable genes across epiblast samples from human embryo extended culture (Xiang et al., 2019) with projection of embryo single cells. (I) FPKM values for naïve-formative specific genes in naïve, formative or conventional hPSCs. (J) Boxplots of naïve-formative specific gene expression in human epiblast stages and primitive streak anlage (PSA). (K) Heatmap of differentially expressed transposable elements between naïve, formative and conventional samples. (L) Morphology of FS cells derived directly from human embryo. Scale bar, 100μm. (M) Immunostaining of OCT4, SOX2 and NANOG in embryo-derived hFS cells. Scale bar, 250μm (N) RT-qPCR analysis of embryo-derived hFS cells. Error bars represent S.D. from technical duplicates.

Star Methods

CONTACT FOR REAGENT AND RESOURCE SHARING

Lead Contact

Further information and requests for resources and reagents should be directed to and will be fulfilled by the Lead Contact, Austin Smith (austin.smith@exeter.ac.uk).

Materials Availability

All stable reagents generated in this study are available from the Lead Contact without restriction except for human embryo derived cell lines for which permission must be requested from UK Stem Cell Steering Committee and a Materials Transfer Agreement completed.

Data and Code

The datasets reported in this paper are deposited in GEO with the following accession codes: RNA-seq and ATAC-seq, GSE131556; scRNA-seq, GSE156589; ChIP-seq, GSE156261

EXPERIMENTAL MODEL AND SUBJECT DETAILS

Mice

Mice used in these studies were adult females aged 6-10 weeks. CD1 and 129aa strains provided embryos for cell line derivation and ROSA$^{mT/mG}$ mice provided donor embryos for primary epiblast injections. Host embryos for chimaera generation were from C57BL/6. CBA/BL6 F1 animals were used as transfer recipients. Animals in the facility tested positive for *Helicobacter* and negative for other specific pathogens. Studies were carried out in a UK Home Office designated facility in accordance with EU guidelines for the care and use of laboratory animals, and under authority of UK Home Office project licence 76777883. Use of animals in this project was approved by the Animal Welfare and Ethical Review Body for the University of Cambridge.

Human Embryos

Supernumerary frozen human embryos were donated with informed consent by couples undergoing in vitro fertility treatment. Use of human embryos in this research is approved by the Multi-Centre Research Ethics Committee, approval O4/MRE03/44, and licensed by the Human Embryology & Fertilisation Authority of the United Kingdom, research license R0178.

Cell Cultures

Cell lines are listed in the Key Resources Table. Cell lines were cultured without antibiotics in humidified incubators at 37˚C in 7% CO_2. Reduced oxygen (5%) was used except for mouse ES cells, which were maintained in atmospheric oxygen. Cell lines tested negative for mycoplasma by periodic PCR screening.

Mouse FS cell, EpiSC and ES cell culture

FS cells were cultured in A_{lo}XR medium, comprising 3ng/ml of activin A, 2μM XAV939 and 1.0μM BMS439 in N2B27 medium (Nichols and Ying, 2006). EpiSCs were cultured in either AF

(20ng/ml activin A and 12.5ng/ml Fgf2) or AFX (20ng/ml activin A, 12.5ng/ml Fgf2 and 2μM XAV939) in N2B27 medium. When passaging, cells were dissociated by Accutase into clumps and re-plated every 2-3 days at a ratio of 1:10-1:20. Mouse ES cells were maintained in 2i/LIF medium as described (Mulas et al., 2019). FS cells and EpiSCs were maintained on fibronectin (Fn) coated (16.7 μg/ml) plates. Experiments were generally performed between p10 and p30.

Derivation of FS and EpiSCs from mouse embryo

E5.5 mouse embryos were dissected from decidua and further micro-dissected into embryonic and extraembryonic parts. Extra-embryonic endoderm layers were removed by mouth pipette and individual epiblasts were plated onto Fn coated (16.7 μg/ml) 4-well plates in either FS or EpiSC medium. After the epiblast outgrowth became large enough, the outgrowth was briefly incubated in Accutase and collected in wash buffer and re-plated onto a fresh 4-well plate.

Derivation of FS and EpiSCs from mouse ES cells

ES cells were plated either directly in A_{lo}XR, AF or AFX medium or N2B27 basal medium for two days and then re-plated in A_{lo}XR, AF or AFX medium. Cultures were passaged at higher densities for the first 4-5 passages with Accutase.

Derivation of human FS cells from naïve PSCs

Human naïve PSC propagated in PXGL (Bredenkamp et al., 2019) were cultured in N2B27 medium for 7 days before changing to A_{lo}XR. Cells were passaged every 3-5 days at a ratio of 1:10-1:20 and Rock inhibitor was added for the first 24 hours after dissociation. hFS cells were cultured on plates pre-coated with Laminin (10 μg/ml) and Fn (16.7 μg/ml).

Derivation of human FS cell from embryos

Day 5 or day 6 human embryos were thawed using SAGE REF ART 8030 vitrification warming kit as per the manufacturer's instructions and cultured for one or two days in N2B27 basal medium in 7% CO_2 and 5% O_2 at 37˚C. ICMs were isolated on the following day by immunosurgery (Solter and Knowles, 1975) or mechanical dissociation and plated in A_{lo}XR in the presence of Rock inhibitor on laminin/Fn coated 4-well plates. 2-4 weeks later, outgrowths were mechanically dissociated into clumps and replated into a fresh well. After this initial passage, Accutase was used for routine passaging.

METHODS DETAILS

Embryoid body differentiation

2,000 cells were plated in low-binding 96-well plates in GMEM supplemented with 10% fetal calf serum, 2 mM L-glutamine, 0.1mM Non-essential Amino Acid (NEAA) (GIBCO), 1mM Sodium Pyruvate and 0.1mM 2-ME. After 5 days, the EBs were transferred for outgrowth onto gelatin-coated plates in fresh medium.

PGCLC differentiation

3,000 cells were plated in low-binding 96-well plates in GK15 medium (GMEM and 15 % Knockout Serum Replacement (GIBCO), 0.1 mM NEAA (GIBCO), 1mM Sodium Pyruvate, 2mM L-Glutamine, 0.1mM 2-mercaptoethanol) supplemented with 500 ng/ml BMP2, 100ng/ml mSCF, 1μg/ml hLIF, 50ng/ml EGF in the presence of 10μM Rho-associated kinase inhibitor Y27632.

Mesoderm induction
Mouse FS cells were plated with 20ng/ml activin A and 3μM CH in N2B27 for 48 hours on Fn coated plates. Human FS cells were plated with 3μM CHIR99021 and 500 nM LDN193189 for the first 2 days followed by the addition of 20ng/ml of Fgf2 from day 3 to day 6.

Endoderm induction
Mouse FS cells were plated with 20ng/ml activin A and 3 μM CH in N2B27 for 24 hours and the medium was replaced thereafter with 20ng/ml of activin A only for a further 2 days on Fn coated plate. Human FS cells were differentiated in 100ng/ml activin A, 100nM PI-103, 3μM CH, 10ng/ml Fgf2, 3ng/ml BMP4 and 10μg/ml Heparin for the first 24hrs and then replaced with 100ng/ml activin A, 100nM PI-103, 20ng/ml Fgf2, 250nM LDN193189 and 10 μg/ml Heparin for a further 2 days.

Neural induction
Mouse FS cells were plated on laminin coated plates in N2B27 (Mulas et al., 2019). Human FS cells were plated with 1μM A83-01 and 500nM LDN193189.

Signal responsiveness
Cells were plated in self-renewal medium and cultured overnight. On the following day, medium was changed to N2B27 medium with or without growth factors/inhibitors. The concentrations used were, activin A (20 ng/ml), Fgf2 (12.5 ng/ml), CHIR99021 (CH, 3μM), Bmp2 (10 ng/ml), XAV939 (2 μM).

Flow cytometry analysis
Mouse endoderm and mesoderm cells were dissociated with Cell Dissociation Buffer (GIBCO). mPGCLC were dissociated with TripLE Express (GIBCO). After the dissociation, cells were incubated with fluorophore-conjugated antibodies in rat serum on ice for 20 min. Cells were washed once with wash buffer and analysed in HANK's buffer supplemented with 1 % BSA. Antibodies are listed in the Key Resource table.

RT-qPCR
Total RNAs were purified by Reliaprep RNA miniprep kit (Promega). cDNAs were prepared by GoScript reverse transcription system (Promega). PCR was performed by Taqman Gene Expression Master Mix (Thermo Fisher Scientific) with Taqman (Thermo Fisher Scientific) or Universal Probe Library (Roche) probes. Probes and primer information are listed in Table S3.

Immunofluorescence analysis
Cells were fixed on plates in 4% PFA for 15 minutes at RT. Cell were blocked with 5% skimmed milk or BSA/PBS 0.1 % TritonX. Primary and secondary antibodies were incubated for 1 hour at RT or overnight at 4˚C. Antibodies used were listed in key resource table. Cells were imaged by LeicaDMI4000. PGCLCs and embryo sections were imaged by Leica SP5.

FISH for *Xist*
FS cells were plated on Fn coated glass slide (Roboz Surgical instrument). The fluorescent conjugated RNA probe was purchased from Stellaris (Biosearch Technologies). *Xist* FSIH was performed as described previously (Sousa et al., 2018). Nuclear was stained with Dapi and imaged by Eclipse Ti Spinning Disk confocal microscope (Nikon).

Metaphase chromosome analysis
FS Cells were treated with KaryoMAX colcemid (Gibco) and cultured further 2.5 hours. Cells were washed with PBS and harvested by Accutase and collected in wash buffer. After centrifuge, cells were resuspended in 5 ml of pre-warmed 0.075M KCl and incubated for 15 minutes at RT. Freshly prepared ice cold fixative solution (methanol: glacial acetic acid (3:1)) (100 µl) were added into the suspension and centrifuge. Cells were resuspended in 250-500 µl of fixative solution and up to 20 µl was spread onto a glass slide. DNA was counterstained with DAPI and spreads were imaged by Leica DMI4000 for counting. Karyotype analysis of embryo derived hFS cell lines were performed by Medical Genetics Service, Cytogenetics Laboratory, Cambridge University Hospitals.

Immunoblotting
Culture plates were taken out from the incubator and placed on ice. Cells were washed with ice-cold PBS and lysed with RIPA buffer in the presence of Protease/Phosphatase inhibitor cocktail (Invitrogen). Lysed cells were rotated for 20 minutes and sonicated in Bioruptor (Diagenode). Cell lysates were cleared by centrifugation, and the supernatant was recovered. Protein concentrations were measured by the BCA method (Pierce). 25 µg of protein was loaded in each well. Blots were blocked with 5% BSA/TBS 0.1 % Triton-X for 1 hour at RT and incubated overnight with primary antibodies at 4˚C. Secondary antibodies were incubated for 1 hour at RT and signals were detected with ECL Select (GE Healthcare) and Odyssey Fc (Li-Cor). NaOH (0.2N) was used for stripping.

***Etv4/5* and *Otx2* knock out analysis**
Etv4/5 dKO ES cell lines were established from Etv4 KO ES cells (Kalkan et al., 2019) using a CRISPR/Cas9 based method. gRNAs were designed to excise Ets domain of Etv5 in Exon13 and Exon15. *Otx2* KO ES cell lines were established from E14tg2a ES cells. gRNAs were designed to excise homeobox in Exon3. gRNAs were cloned into pCML32. Targeted ES cell clones were picked and genotyped by genomic PCR. Oct4 and Otx2 KO in FS cells were performed by co-transfected with one gRNA expression plasmid (pCML32, Oct4-1, Otx2-1 in Table S3, puromycin resistance, *piggyBac* vector) with Cas9 expressing plasmid (G418 resistance, *piggybac* vector) and PBase expressing plasmid by TransIT LT1 (Mirus). Transfected cells were selected with 1 µg/ml of puromycin and 250 µg/ml of G418 from 24-48 hours post-transfection. Cells were counted and re-plated for another three days to form colonies. Rock inhibitor was added for the first 24 hours after replating. Alkaline phosphatase staining was performed following manufacture's instruction (Sigma-Aldrich). gRNA sequences, genotyping primers and the amplicon sizes of each genotypes are listed in Table S3.

RNA-sequencing
For the bulk RNA-sequencing experiment, cells were lysed in Trizol (Thermo Fisher Scientific) and total RNAs were prepared using the PureLink RNA Mini Kit (Thermo Fisher Scientific). Ribosomal RNAs were removed by Ribo-Zero rRNA Removal Kit (Illumina) and libraries were constructed using the NEXTflex Rapid Directional RNA-seq Kit (Bioo Scientific). For the low-input RNA-sequencing experiment, RNA was isolated from cells and epiblasts with the PicoPure RNA Isolation kit (Thermo Fisher Scientific) and libraries were constructed using the SMARTerR Stranded Total RNA-Seq Kit v2- Pico InputMammalian (Takara Clontech). 1,000 FS cells and isolated entire single epiblasts from E5.0, E5.5, E6.0 embryos were used per sample.

ATAC-seq

50,000 cells were collected and washed with ice-cold PBS once then lysed in lysis buffer (10 mM Tris-HCl, pH 7.4, 10 mM NaCl, 3 mM $MgCl_2$, 0.1% IGEPAL). The nuclear pellets were collected and Tn5 tagmentation and library construction performed using the Illumina Nextera kit (FC-121-1030). DNA was purified with AMPure XP beads (Beckman Coulter).

ChIP-seq

ChIP was performed following the protocol reported previously (Kalkan et al., 2019). Briefly, chromatin was cross-linked with 1% formaldehyde for 10 minutes at RT and quenched with 125 mM Glycine for 5 minutes at RT with rotation. After cell pellets were lysed, sonication was performed for 16 cycles on High setting, 30sec ON/30 sec OFF cycle by Bioruptor (Diagenode), $2x10^7$ cells per 300 µl in Bioruptor tube. 10% inputs were collected for the later library construction. Chromatin was immunoprecipitated with 2 µg of each antibodies and 20 µl of Protein G Dynabeads (Invitrogen) were used against $3x10^6$ cells. After the washes, DNA was eluted and each samples were treated with 2.5 µg/ml RNase A at 37˚C for 30 minutes followed by 87.5 µg/ml Proteinase K at 55˚C for 1 hour. DNA was purified with PCR clean-up kit (Qiagen). Libraries were prepared by NEXTflex Rapid DNA-Seq Kit 2.0 bundle with 96 HT barcodes (ParkinElmer).

Single-cell RNA-seq

Cells were directly sorted into each well of 96-well plate filled with 2.3 µl of lysis buffer (1 unit/µl of SUPERaseIN RNase inhibitor (Invitrogen), 0.2 % Triton X) by BD FACSAria Fusion (BD Biosciences). Libraries were prepared using the Smart-seq2 protocol (Illumina) (Picelli et al., 2014).

Chimaeras

FS cell chimaeras

FS cells were pre-treated with 10 µM Rock inhibitor for 1 hour before harvesting. Around 10 singly dissociated cells were injected into each blastocyst stage embryo. Embryos are either transferred into pseudo-pregnant mice or cultured *in vitro* for another 24 hours in N2B27. E9.5 mid-gestation stage embryos and juvenile mouse tissues were imaged by Leica stereo microscope. For sectioning, embryos and E12.5 gonads were replaced with 20% sucrose/PBS overnight at 4˚C after the fixation then embedded in OCT compound and sectioned at 8 µm thickness. Sections were imaged by Zeiss apotome microscope or Leica SP5 confocal microscope.

Epiblast chimaeras

Homozygous mTmG mice were crossed with CD1 mice to obtain embryos. E5.5, 6.0-6.25 and E6.5 embryos were dissected from decidua and separated into embryonic and extraembryonic halves. Extraembryonic endoderm layers were removed using a mouth-controlled pulled Pasteur pipette. Isolated epiblasts were treated with Accutase at room temperature and washed with M2 medium in the presence of 10 µM Rock inhibitor. Ten dissociated cells were injected per E3.5 blastocyst stage embryo of strain C57BL/6. Microinjection was performed in M2 medium containing Rock inhibitor. For sectioning, embryos were embedded in OCT compound and sectioned at 10µm thickness. Sections were stained with anti-RFP antibody and imaged using a Leica DMI4000.

QUANTIFICATION AND STATISTICAL ANALYSIS

Bulk RNA-seq analysis

Low-quality RNA-seq reads and adaptor sequences were removed using *Trim Galore!*. Reads were aligned to the mouse (GRCm38/mm10) and human (GRCh38/hg38) reference genomes using *TopHat2* with parameters " –read-mismatch 2 –max-multihits 1 –b2-sensitive" considering uniquely mapping reads only. Gene counts were obtained using *featureCounts* using ENSEMBL (release 89) gene annotations. Normalization and differential expression analyses were performed using the R/Bioconductor *DESeq2* package. Normalized counts were transformed into log2 fragments per million (FPKM). Genes with log2 fold change>1.6 and adjusted p-value <0.05 were considered differentially expressed. Differentially expressed gene clusters for human cells were identified by k-means clustering of the first five principal components using the R '*kmeans*' function. The distance plot was calculated using Euclidean distance between samples based on log2 normalized counts of expression values. Heatmaps were generated using the R '*pheatmap*" function.

For transposable elements (Tes), reads were aligned to the human (GRCh38/hg38) reference genome using *bowtie* with parameters "-a –best –strata -m 1 -v 2", retaining uniquely mapping reads only in order to identify the genomic origin of TE transcription. Read counts on Tes were obtained using *featureCounts* on UCSC RepeatMasker-annotated regions. Normalization and differential expression analyses between cell types of identical genotype were performed with the R/Bioconductor *DESeq* package. Tes with an expression of at least log2-normalized counts > 3.5 in any cell type, a log2 fold change>2 and an adjusted p-value <0.05 were considered differentially expressed.

Published RNA-seq data comparison analysis

Mouse single cell RNA-seq data was downloaded from Nakamura et al., 2016 (GEO: GSE74767). Human naïve and conventional PSC transcriptome data were downloaded from SRA: SRP104789, ENA:E-MTAB-5114, ENA:E-MTAB-5674, GEO:GSE123005. The data was processed using the same methods as described above, except that genes with zero counts were removed from the single cell RNA-seq data matrix before further processing by DESeq2. The matrix of log2 fragment per millions for the *Macaca fascicularis* was obtained from GEO: GSE74767 (Nakamura et al., 2016). The Human single cell RNA-seq FPKM 24ummarized counts matrix was downloaded from GEO: GSE136447 (Xiang et al., 2019).

PCA plots

Principal component analyses (PCA) were performed using the R '*prcomp*' function based on log2-transformed Z-score expression values. To compare mouse and human bulk RNA-seq with mouse and macaque single cell RNA-seq, the principal components of the single cell RNA-seq data were calculated, with the bulk RNA-seq data projected onto this PCA space using the R '*predict'* function. These PCAs were computed using all expressed genes or with genes differentially expressed between the formative and primed lines in order to narrow down genes important for developmental progression. To compare human bulk RNA-seq with human single cell RNA-seq data, Log2 transformed counts were used. Using the most variable genes across the single cell stages, a PCA of the bulk samples was computed and the single cells were projected using the R '*predict*' function.

scRNA-seq analysis

Raw files were quality controlled using FastQC v0.11.3 and results 25ummarized with MultiQC, with checks including distributions of nucleotide content and sequencing depth. Reads were aligned to the *M.musculus* GRCm38.p6 reference genome with Ensembl v98 annotations using STAR v2.7.3a (--outSAMtype BAM SortedByCoordinate). Protein-coding gene quantification was done using Subread featureCounts v2.0.0 with Ensembl v98 annotations; only uniquely mapped reads were used. Cells with fewer than 3M reads were removed from further analysis, leaving 326 cells that passed the threshold. Raw expression levels were normalized using sctransform (Hafemeister and Satija, 2019), and the PCA created using the 2000 most abundant genes across the data. Jaccard similarity indices were calculated on the 2000 most abundant genes per cell, with similarities calculated between all cells of the same type.

GO-terms

Gene ontology (GO) term enrichment analyses were performed using the *David* tool.

ATAC-seq

Reads were quality-trimmed using *Trim Galore!*, and reads shorter than 15 nt were discarded. Reads were aligned to the mouse reference genome (GRCm38/mm10) using *bowtie* with parameters "-m1 -v1 –best –strata -X 2000 –trim3 1". Duplicates were removed using *Picard tools*. Reads longer than one nucleosome length (146 nt) were discarded, and an offset of 4 nts was introduced. Peaks were called with *MACS2* and parameters "–nomodel –shift -55 –extsize 110 –broad -g mm –broad-cutoff 0.1". Bigwig files for visualization on the UCSC Genome browser were generated using *deeptools bamcoverage* with parameters "–binSize 10 and –normalizeUsing RPKM". ATAC peaks specific to each cell type were identified using *edgeR* within the R/Bioconductor *DiffBind* package using the option "bNot = T" to allow for contrasts between each cell type against all others. Significant peaks were determined using a log2 fold change of > 1 and FDR < 0.05. Heatmaps of ATAC-seq peaks were generated with *deeptools plotHeatmap*. DNA motif enrichment analyses for cell type-specific ATAC-seq peaks was performed using *HOMER*.

BS-seq

Whole genome BS-seq data was obtained from Zylicz et al., 2014 (GEO: GSE70355**)**. BS-seq reads were aligned to the mouse reference genome (GRCm38/mm10) and deduplicated using *Bismark*. *MethPipe* was used calculate methylation levels at each CpG, and only CpGs with at least 5X read coverage were retained for further analyses. Methylation levels were averaged using a 250nt-sliding window to generate bigwig files.

ChIP-seq

Raw files were quality controlled using FastQC v0.11.3 and results summarised with MultiQC, with checks including distributions of nucleotide content, sequencing depth and adapter contamination. Reads were aligned to the *M.musculus* GRCm38.p6 reference genome using bwa mem v0.7.10-r789 (default parameters); the MT, X, Y chromosomes and scaffolds were excluded from the resulting BAM files. Genome browser tracks for the UCSC genome browser were created with deepTools bamCoverage v3.3.1 (—binSize 30). Averaged genome browser tracks for ChIP profile visualization were created as follows: first the tracks were generated with bamCoverage (—binSize 5 –normalizeUsing RPKM), then the output was averaged using

wiggletools v1.2.1 (Zerbino et al., 2014). Profiles of the ChIP tracks on the ATAC peaks were created using deepTools computeMatrix (reference-point --binSize 5 -b 4000 -a 4000 --referencePoint center) and plotProfile (default parameters). To identify bivalent promoters, peak regions were called with macs2 v2.2.6 (-f BAMPE -q 0.05), only peaks with signalValue>5 were considered for downstream analysis. Peak regions were intersected per condition and across histone marks using bedops v2.4.38. HOMER v4.10 was used to calculate distance between peaks and transcription start sites (mm10 -size 3000); peaks within 3kb of a TSS were considered as promoter peaks.

KEY RESOURCES TABLE

REAGENT or RESOURCE	SOURCE	IDENTIFIER
Antibodies		
Mouse monoclonal anti-Oct3/4 (C-10)	Santa Cruz	Cat#SC-5279; RRID:AB_628051
Goat polyclonal anti-Oct3/4 (N-19)	Santa Cruz	Cat#SC-8628; RRID:AB_653551
Goat polyclonal anti-Brachyury	R&D systems	Cat#AF2085; RRID:AB_2200235
Rabbit polyclonal anti-Sox1	Cell Signaling Technology	Cat#4194; RRID:AB_1904140
Rabbit polyclonal anti-Stella/Dppa3	Abcam	Cat#ab19878; RRID:AB_2246120
Rat monoclonal anti-Blimp1/Prdm1	Santa Cruz	Cat#SC-47732; RRID:AB_628168
Mouse monoclonal anti-Foxa2	Abnova	Cat#H00003170-M10; RRID:AB_534871
Mouse monoclonal anti-Tuj1	R&D systems	Cat#MAB1195; RRID:AB_357520
Mouse anti-cardiac Troponin T (1C11)	Abcam	Cat#Ab8295; RRID:AB_306445
Goat polyclonal anti-Sox17	R&D systems	Cat#AF1924; RRID:AB_355060
Goat polyclonal anti-Gata4	Santa Cruz	Cat#SC-1237; RRID:AB_2108747
Rabbit polyclonal anti-Eomes	Abcam	Cat#ab23345; RRID:AB_778267
Rat monoclonal anti-Ecadherin (ECCD2)	Kind gift from Prof. M Takeichi	N/A
Rat monoclonal anti-Nanog	eBioscience	Cat#14-5761-80; RRID:AB_763613
Rat monoclonal anti-Sox2	eBioscience	Cat#14-9811-82; RRID:AB_11219471
Mouse monoclonal anti-Oct6 (Pou3f1)	Miilipore	Cat#MABN738; RRID:AB_2876862
Rabbit polyclonal anti-mKusabira Orange	MBL	Cat#PM051M; RRID:AB_2876863
Alexa Fluore 647 anti-SSEA1	BD Bioscience	Cat#562277; RRID:AB_11154583
PE Anti-mouse/rat CD61	Biolegend	Cat#104307; RRID:AB_313084
Anti-CD324 (Ecadherin) eFluor-660	eBioscience	Cat#50-3249-82; RRID:AB_11040003
PE-Cy7 Anti-Ecadherin	Biolegend	Cat#147310; RRID:AB_2564188

APC Anti-mouse CD184 (Cxcr4)	Biolegend	Cat#146508; RRID:AB_2562785
PE Anti-Flk1	Biolegend	Cat#136403; RRID:AB_1967093
Rabbit anti-RFP	Rockland	Cat#600-401-379; RRID:AB_2209751
Rabbit anti-mvh	Abcam	Cat#ab13840; RRID:AB443012
Rabbit anti-phospho Smad2	Cell Signaling Technologies	Cat#3108; RRID:AB_490941
Mouse anti-total Smad2/3	BD Bioscience	Cat#610842; RRID:AB_398161
Mouse anti-Gapdh	Sigma-Aldrich	Cat#G8795; RRID:AB_1078991
Rabbit anti-H3K4me1	Abcam	Cat#ab8895; RRID:AB_306847
Rabbit anti-H3K4me3	Diagenode	Cat#C15410003; RRID:AB_2616052
Rabbit anti-H3K27Ac	Active Motif	Cat#39135; RRID:AB_2614979
Rabbit anti-H3K27me3	Merck	Cat#07-449; RRID:AB_310624
Bacterial and Virus Strains		
Biological Samples		
Chemicals, Peptides, and Recombinant Proteins		
XAV939	Sigma Aldrich	X-3004
BMS493	Tocris Bio-Techne	3509
A83-01	Generon	A12358-50
SB-505124	Selleckchem	S2186
LDN193189	Axon Medchem	Axon 1509
PD0325901	abcr	AB 253775
CHIR99021	abcr	AB 253776
Y27632	Millipore	Cat 688000
Recombinant Mouse LIF	In house	N/A
Recombinant human LIF	In House	N/A
Recombinant human activin A	Qkine	Qk005
Recombinant zebrafish Fgf2	Qkine	Qk002
Recombinant mouse Stem Cell Factor	BioLegend	579706
Recombinant human BMP2	In House	N/A
N2 Supplement	In house	N/A
B27 Supplement	Thermo Fisher Scientific	17504044
Neurobasal	Thermo Fisher Scientific	11540566
DMEM/F12	Thermo Fisher Scientific	21103049
Human Plasma Fibronectin	Millipore	FC010
Tissue culture Laminin	Millipore	CC095-5MG
Gelatin	Sigma-Aldrich	G-1890
Accutase	Biolegend	423201
M2 medium	Sigma-Aldrich	M-7167

Critical Commercial Assays		
NEXTflex Rapid Directional RNA-seq Kit	Bioo Scientific	5138-08
Ribo-Zero rRNA Removal Kit	Illumina	MRZH11124
PureLink RNA Mini kit	Thermo Fisher Scientific	12183018A
PicoPure RNA Isolation kit	Thermo Fisher Scientific	KIT0214
SMARTerR Stranded Total RNA-Seq Kit v2 – Pico InputMammalian	Takara Clontech	634412
Nextera DNA Library Preparation Kit	Illumina	FC-121-1030
SAGE Warming Kit	CooperSurgical Fertility & Genomic Solutions	ART-8030
NEXTflex Rapid DNA-Seq Kit 2.0 bundle with 96 HT barcodes	PerkinElmer	NOVA-5188-13
Mouse Xist Stellaris RNA FISH Probe with Quasar 670 Dye	BioSearch Technologies	VSMF-3095-5
10 CIRCLE, 7MM ID, FROSTED, HEAVY TEFLON COATED Slide	Roboz Surgical Instrument	F107-HTC
TransIT LT1	Mirus	MIR2304
Alkaline Phaphatase Kit	Sigma Aldrich	86R-1KIT
Deposited Data		
RNA-seq	This paper	GSE131566
ATAC-seq	This paper	GSE131566
scRNA-seq	This paper	GSE156589
ChIP-seq	This paper	GSE156261
Experimental Models: Cell Lines		
5ar1 (mFS)	This paper	
5ar2 (mFS)	This paper	
5ar3 (mFS)	This paper	
5ar5 (mFS)	This paper	
5cdr1 (mFS)	This paper	
5cdr2 (mFS)	This paper	
NBRA3.2 (mFS)	This paper	
5a6 (mFS)	This paper	
E14Tg2a (mES)	Hooper et al 1987	
Rd2 (mES)	Kalkan et al 2017	
Sox1::GFP (mES)	Starvridis et al 2003	
AFX6 (mEpiSC)	This paper	
AFX33 (mEpiSC)	This paper	
AF32 (mEpiSC)	This paper	
OEC2 (mEpiSC)	Guo et al 2009	
HNES1 (hES)	Guo et al 2016	
cR-H9 (hES)	Guo et al 2017	
cR-Shef6 (hES)	Guo et al 2017	
Etv4/5 dKO ES	This paper	
Otx2 KO ES	This paper	

hFS1	This paper	
hFS2	This paper	
hFS3	This paper	
Experimental Models: Organisms/Strains		
Mouse/CD-1	Charles River	022
Mouse/129aa	WT-Gurdon Institute	N/A
Mouse/ ROSA$^{mT/mG}$	Jackson Laboratory	007576
Mouse/C57BL/6	WT-Gurdon Institute	N/A
Oligonucleotides		
gRNA sequences	See Table S3	N/A
Genotyping primers	See Table S3	N/A
Taqman probes and UPL primers for qRT-PCR	See Table S3	N/A
Recombinant DNA		
pPBCAG-mKO2-IP	This paper	N/A
pPBCAG-GFP-IP	This paper	N/A
pPBCAG-Cas9-IN	This paper	N/A
pCML32	This paper	N/A
Software and Algorithms		
Tophat2 v2.1.0	Kim et al, 2013	https://ccb.jhu.edu/software/tophat/index.shtml
TrimGalore v0.4.5	Felix Krueger, 2015	https://www.bioinformatics.babraham.ac.uk/projects/trim_galore/
FeatureCounts v1.5.0	Liao Y, Smyth GK, Shi W, 2019.	http://subread.sourceforge.net/
R v3.6.2	R Core Team, 2017	https://www.R-project.org/
DESeq2 v1.18.1	Love MI, Huber W, Anders S (2014).	https://bioconductor.org/packages/release/bioc/html/DESeq2.html
Pheatmap		https://CRAN.R-project.org/package=pheatmap
ggplot2		https://ggplot2.tidyverse.org/
DeepTools	Ramírez et al., 2016	doi: 10.1093/nar/gkw257
Diffbind v2.6.6	Stark R and Brown G 2011.	https://bioconductor.org/packages/release/bioc/html/DiffBind.html
MACS2	Zhang et al., 2008	
DAVID v6.8	Huang et al. 2009	https://david.ncifcrf.gov/

HOMER v4.10	Heinz et al., 2010	http://homer.ucsd.edu/homer/
Bismark	Krueger F and Andrews SR, 2011	https://www.bioinformatics.babraham.ac.uk/projects/bismark/
MarkDuplicates	Picard tools	
Seurat v3.1.0	Butler et al., 2018	https://satijalab.org/seurat/
STAR v2.7.3a	Dobin et al., 2013	https://github.com/alexdobin/STAR
Wiggletools	Zerbino et al., 2014	https://github.com/Ensembl/WiggleTools
Bowtie	Langmead and Salzberg, 2012	
Samtools v1.9		http://www.htslib.org/
FastQC v0.11.3		https://www.bioinformatics.babraham.ac.uk/projects/fastqc/
MultiQC v1.8		https://multiqc.info/
Methpipe	Song Q, et al., 2013	http://smithlabresearch.org/software/methpipe/
Venny 2.1		https://bioinfogp.cnb.csic.es/tools/venny/index.html
FCS Express 7 Research		De Novo Software
Other		

REFERENCES

Acampora, D., Di Giovannantonio, L.G., and Simeone, A. (2013). Otx2 is an intrinsic determinant of the embryonic stem cell state and is required for transition to a stable epiblast stem cell condition. Development *140*, 43-55.

Acampora, D., Omodei, D., Petrosino, G., Garofalo, A., Savarese, M., Nigro, V., Di Giovannantonio, L.G., Mercadante, V., and Simeone, A. (2016). Loss of the Otx2-Binding Site in the Nanog Promoter Affects the Integrity of Embryonic Stem Cell Subtypes and Specification of Inner Cell Mass-Derived Epiblast. Cell Rep *15*, 2651-2664.

Allison, T.F., Smith, A.J.H., Anastassiadis, K., Sloane-Stanley, J., Biga, V., Stavish, D., Hackland, J., Sabri, S., Langerman, J., Jones, M.*, et al.* (2018). Identification and Single-Cell Functional Characterization of an Endodermally Biased Pluripotent Substate in Human Embryonic Stem Cells. Stem Cell Reports *10*, 1895-1907.

Ang, S.L., Jin, O., Rhinn, M., Daigle, N., Stevenson, L., and Rossant, J. (1996). A targeted mouse Otx2 mutation leads to severe defects in gastrulation and formation of axial mesoderm and to deletion of rostral brain. Development *122*, 243-252.

Auclair, G., Guibert, S., Bender, A., and Weber, M. (2014). Ontogeny of CpG island methylation and specificity of DNMT3 methyltransferases during embryonic development in the mouse. Genome Biol *15*, 545.

Azuara, V., Perry, P., Sauer, S., Spivakov, M., Jorgensen, H.F., John, R.M., Gouti, M., Casanova, M., Warnes, G., Merkenschlager, M.*, et al.* (2006). Chromatin signatures of pluripotent cell lines. Nat Cell Biol *8*, 532-538.

Bain, G., Kitchens, D., Yao, M., Huettner, J.E., and Gottlieb, D.I. (1995). Embryonic stem cells express neuronal properties in vitro. Dev Biol *168*, 342-357.

Beddington, R.S., and Robertson, E.J. (1998). Anterior patterning in mouse. Trends Genet *14*, 277-284.
Bernstein, B.E., Mikkelsen, T.S., Xie, X., Kamal, M., Huebert, D.J., Cuff, J., Fry, B., Meissner, A., Wernig, M., Plath, K.*, et al.* (2006). A bivalent chromatin structure marks key developmental genes in embryonic stem cells. Cell *125*, 315-326.
Boroviak, T., Loos, R., Bertone, P., Smith, A., and Nichols, J. (2014). The ability of inner-cell-mass cells to self-renew as embryonic stem cells is acquired following epiblast specification. Nat Cell Biol *16*, 516-528.
Boroviak, T., Loos, R., Lombard, P., Okahara, J., Behr, R., Sasaki, E., Nichols, J., Smith, A., and Bertone, P. (2015). Lineage-Specific Profiling Delineates the Emergence and Progression of Naive Pluripotency in Mammalian Embryogenesis. Developmental Cell *35*, 366-382.
Bredenkamp, N., Yang, J., Clarke, J., Stirparo, G.G., von Meyenn, F., Dietmann, S., Baker, D., Drummond, R., Ren, Y., Li, D.*, et al.* (2019). Wnt Inhibition Facilitates RNA-Mediated Reprogramming of Human Somatic Cells to Naive Pluripotency. Stem Cell Reports *13*, 1083-1098.
Brennan, J., Lu, C.C., Norris, D.P., Rodriguez, T.A., Beddington, R.S., and Robertson, E.J. (2001). Nodal signalling in the epiblast patterns the early mouse embryo. Nature *411*, 965-969.
Brons, I.G., Smithers, L.E., Trotter, M.W., Rugg-Gunn, P., Sun, B., Chuva de Sousa Lopes, S.M., Howlett, S.K., Clarkson, A., Ahrlund-Richter, L., Pedersen, R.A.*, et al.* (2007). Derivation of pluripotent epiblast stem cells from mammalian embryos. Nature *448*, 191-195.
Brook, F.A., and Gardner, R.L. (1997). The origin and efficient derivation of embryonic stem cells in the mouse. PNAS *94*, 5709-5712.
Buecker, C., Srinivasan, R., Wu, Z., Calo, E., Acampora, D., Faial, T., Simeone, A., Tan, M., Swigut, T., and Wysocka, J. (2014). Reorganization of enhancer patterns in transition from naive to primed pluripotency. Cell Stem Cell *14*, 838-853.
Buenrostro, J.D., Giresi, P.G., Zaba, L.C., Chang, H.Y., and Greenleaf, W.J. (2013). Transposition of native chromatin for fast and sensitive epigenomic profiling of open chromatin, DNA-binding proteins and nucleosome position. Nat Methods *10*, 1213-1218.
Burgold, T., Barber, M., Kloet, S., Cramard, J., Gharbi, S., Floyd, R., Kinoshita, M., Ralser, M., Vermeulen, M., Reynolds, N.*, et al.* (2019). The Nucleosome Remodelling and Deacetylation complex suppresses transcriptional noise during lineage commitment. Embo J.
Chal, J., Al Tanoury, Z., Hestin, M., Gobert, B., Aivio, S., Hick, A., Cherrier, T., Nesmith, A.P., Parker, K.K., and Pourquie, O. (2016). Generation of human muscle fibers and satellite-like cells from human pluripotent stem cells in vitro. Nat Protoc *11*, 1833-1850.
Chambers, S.M., Fasano, C.A., Papapetrou, E.P., Tomishima, M., Sadelain, M., and Studer, L. (2009). Highly efficient neural conversion of human ES and iPS cells by dual inhibition of SMAD signaling. Nat Biotechnol *27*, 275-280.
Chen, G., Gulbranson, D.R., Hou, Z., Bolin, J.M., Ruotti, V., Probasco, M.D., Smuga-Otto, K., Howden, S.E., Diol, N.R., Propson, N.E.*, et al.* (2011). Chemically defined conditions for human iPSC derivation and culture. Nat Methods *8*, 424-429.
Cheng, S., Pei, Y., He, L., Peng, G., Reinius, B., Tam, P.P.L., Jing, N., and Deng, Q. (2019). Single-Cell RNA-Seq Reveals Cellular Heterogeneity of Pluripotency Transition and X Chromosome Dynamics during Early Mouse Development. Cell Rep *26*, 2593-2607.e2593.
Conlon, F.L., Lyons, K.M., Takaesu, N., Barth, K.S., Kispert, A., Herrmann, B., and Robertson, E.J. (1994). A primary requirement for nodal in the formation and maintenance of the primitive streak in the mouse. Development *120*, 1919-1928.
Cornacchia, D., Zhang, C., Zimmer, B., Chung, S.Y., Fan, Y., Soliman, M.A., Tchieu, J., Chambers, S.M., Shah, H., Paull, D.*, et al.* (2019). Lipid Deprivation Induces a Stable, Naive-to-Primed Intermediate State of Pluripotency in Human PSCs. Cell Stem Cell.
D'Aniello, C., Habibi, E., Cermola, F., Paris, D., Russo, F., Fiorenzano, A., Di Napoli, G., Melck, D.J., Cobellis, G., Angelini, C.*, et al.* (2016). Vitamin C and l-Proline Antagonistic Effects Capture Alternative States in the Pluripotency Continuum. Stem Cell Reports.
Davidson, K.C., Mason, E.A., and Pera, M.F. (2015). The pluripotent state in mouse and human. Development *142*, 3090-3099.

Dunn, S.J., Martello, G., Yordanov, B., Emmott, S., and Smith, A.G. (2014). Defining an essential transcription factor program for naïve pluripotency. Science *344*, 1156-1160.
Friedli, M., and Trono, D. (2015). The Developmental Control of Transposable Elements and the Evolution of Higher Species. Annu Rev Cell Dev Biol *31*, 429-451.
Gardner, R.L. (1985). Clonal analysis of early mammalian development. PhilTransRSoc,B *312*, 163-178.
Gardner, R.L., and Brook, F.A. (1997). Reflections on the biology of embryonic stem cells. Int J Dev Biol *41*, 235-243.
Gardner, R.L., Lyon, M.F., Evans, E.P., and Burtenshaw, M.D. (1985). Clonal analysis of X-chromosome inactivation and the origin of the germ line in the mouse embryo. J Embryol Exp Morphol *88*, 349-363.
Gokhale, P.J., Au-Young, J.K., Dadi, S., Keys, D.N., Harrison, N.J., Jones, M., Soneji, S., Enver, T., Sherlock, J.K., and Andrews, P.W. (2015). Culture adaptation alters transcriptional hierarchies among single human embryonic stem cells reflecting altered patterns of differentiation. PLoS One *10*, e0123467.
Guo, G., von Meyenn, F., Rostovskaya, M., Clarke, J., Dietmann, S., Baker, D., Sahakyan, A., Myers, S., Bertone, P., Reik, W.*, et al.* (2017). Epigenetic resetting of human pluripotency. Development *144*, 2748-2763.
Guo, G., von Meyenn, F., Santos, F., Chen, Y., Reik, W., Bertone, P., Smith, A., and Nichols, J. (2016). Naive Pluripotent Stem Cells Derived Directly from Isolated Cells of the Human Inner Cell Mass. Stem Cell Reports *6*, 437-446.
Guo, G., Yang, J., Nichols, J., Hall, J.S., Eyres, I., Mansfield, W., and Smith, A. (2009). Klf4 reverts developmentally programmed restriction of ground state pluripotency. Development *136*, 1063-1069.
Guzman-Ayala, M., Ben-Haim, N., Beck, S., and Constam, D.B. (2004). Nodal protein processing and fibroblast growth factor 4 synergize to maintain a trophoblast stem cell microenvironment. Proc Natl Acad Sci U S A *101*, 15656-15660.
Hackett, J.A., and Surani, M.A. (2014). Regulatory principles of pluripotency: from the ground state up. Cell Stem Cell *15*, 416-430.
Hafemeister, C., and Satija, R. (2019). Normalization and variance stabilization of single-cell RNA-seq data using regularized negative binomial regression. Genome Biol *20*, 296.
Han, D.W., Tapia, N., Joo, J.Y., Greber, B., Araúzo-Bravo, M.J., Bernemann, C., Ko, K., Wu, G., Stehling, M., Do, J.T.*, et al.* (2010). Epiblast Stem Cell Subpopulations Represent Mouse Embryos of Distinct Pregastrulation Stages. Cell *143*, 617-627.
Haub, O., and Goldfarb, M. (1991). Expression of the fibroblast growth factor-5 gene in the mouse embryo. Development *112*, 397-406.
Hayashi, K., Ohta, H., Kurimoto, K., Aramaki, S., and Saitou, M. (2011). Reconstitution of the mouse germ cell specification pathway in culture by pluripotent stem cells. Cell *146*, 519-532.
Heinz, S., Benner, C., Spann, N., Bertolino, E., Lin, Y.C., Laslo, P., Cheng, J.X., Murre, C., Singh, H., and Glass, C.K. (2010). Simple combinations of lineage-determining transcription factors prime cis-regulatory elements required for macrophage and B cell identities. Mol Cell *38*, 576-589.
Hough, S.R., Laslett, A.L., Grimmond, S.B., Kolle, G., and Pera, M.F. (2009). A continuum of cell states spans pluripotency and lineage commitment in human embryonic stem cells. PLoS One *4*, e7708.
Hough, S.R., Thornton, M., Mason, E., Mar, J.C., Wells, C.A., and Pera, M.F. (2014). Single-cell gene expression profiles define self-renewing, pluripotent, and lineage primed states of human pluripotent stem cells. Stem Cell Reports *2*, 881-895.
Irie, N., Weinberger, L., Tang, W.W., Kobayashi, T., Viukov, S., Manor, Y.S., Dietmann, S., Hanna, J.H., and Surani, M.A. (2015). SOX17 is a critical specifier of human primordial germ cell fate. Cell *160*, 253-268.
Kalkan, T., Bornelöv, S., Mulas, C., Diamanti, E., Lohoff, T., Ralser, M., Middelkamp, S., Lombard, P., Nichols, J., and Smith, A. (2019). Complementary Activity of ETV5, RBPJ, and TCF3 Drives Formative Transition from Naive Pluripotency. Cell Stem Cell *24*, 785-801.e787.

Kalkan, T., Olova, N., Roode, M., Mulas, C., Lee, H.J., Nett, I., Marks, H., Walker, R., Stunnenberg, H.G., Lilley, K.S.*, et al.* (2017). Tracking the embryonic stem cell transition from ground state pluripotency. Development *144*, 1221-1234.
Kalkan, T., and Smith, A. (2014). Mapping the route from naive pluripotency to lineage specification. Phil Trans R Soc B *369*.
Kinoshita, M., and Smith, A. (2018). Pluripotency Deconstructed. Dev Growth Differ *60*, 44-52.
Kojima, Y., Kaufman-Francis, K., Studdert, J.B., Steiner, K.A., Power, M.D., Loebel, D.A., Jones, V., Hor, A., de Alencastro, G., Logan, G.J.*, et al.* (2014). The transcriptional and functional properties of mouse epiblast stem cells resemble the anterior primitive streak. Cell Stem Cell *14*, 107-120.
Kunath, T., Saba-El-Leil, M.K., Almousailleakh, M., Wray, J., Meloche, S., and Smith, A. (2007). FGF stimulation of the Erk1/2 signalling cascade triggers transition of pluripotent embryonic stem cells from self-renewal to lineage commitment. Development *134*, 2895-2902.
Kurek, D., Neagu, A., Tastemel, M., Tuysuz, N., Lehmann, J., van de Werken, H.J., Philipsen, S., van der Linden, R., Maas, A., van, I.W.F.*, et al.* (2015). Endogenous WNT signals mediate BMP-induced and spontaneous differentiation of epiblast stem cells and human embryonic stem cells. Stem Cell Reports *4*, 114-128.
Lau, K.X., Mason, E.A., Kie, J., De Souza, D.P., Kloehn, J., Tull, D., McConville, M.J., Keniry, A., Beck, T., Blewitt, M.E.*, et al.* (2020). Unique properties of a subset of human pluripotent stem cells with high capacity for self-renewal. Nat Commun *11*, 2420.
Lawson, K.A., Meneses, J.J., and Pedersen, R.A. (1991). Clonal analysis of epiblast fate during germ layer formation in the mouse embryo. Development *113*, 891-911.
Liu, P., Wakamiya, M., Shea, M.J., Albrecht, U., Behringer, R.R., and Bradley, A. (1999). Requirement for Wnt3 in vertebrate axis formation. Nat Genet *22*, 361-365.
Loh, K.M., Ang, L.T., Zhang, J., Kumar, V., Ang, J., Auyeong, J.Q., Lee, K.L., Choo, S.H., Lim, C.Y., Nichane, M.*, et al.* (2014). Efficient endoderm induction from human pluripotent stem cells by logically directing signals controlling lineage bifurcations. Cell Stem Cell *14*, 237-252.
Lu, B.C., Cebrian, C., Chi, X., Kuure, S., Kuo, R., Bates, C.M., Arber, S., Hassell, J., MacNeil, L., Hoshi, M.*, et al.* (2009). Etv4 and Etv5 are required downstream of GDNF and Ret for kidney branching morphogenesis. Nat Genet *41*, 1295-1302.
Mak, W., Nesterova, T.B., de Napoles, M., Appanah, R., Yamanaka, S., Otte, A.P., and Brockdorff, N. (2004). Reactivation of the paternal X chromosome in early mouse embryos. Science *303*, 666-669.
Masaki, H., Kato-Itoh, M., Takahashi, Y., Umino, A., Sato, H., Ito, K., Yanagida, A., Nishimura, T., Yamaguchi, T., Hirabayashi, M.*, et al.* (2016). Inhibition of Apoptosis Overcomes Stage-Related Compatibility Barriers to Chimera Formation in Mouse Embryos. Cell Stem Cell *19*, 587-592.
Mesnard, D., Guzman-Ayala, M., and Constam, D.B. (2006). Nodal specifies embryonic visceral endoderm and sustains pluripotent cells in the epiblast before overt axial patterning. Development *133*, 2497-2505.
Mulas, C., Kalkan, T., and Smith, A. (2017). NODAL Secures Pluripotency upon Embryonic Stem Cell Progression from the Ground State. Stem Cell Reports *9*, 77-91.
Mulas, C., Kalkan, T., von Meyenn, F., Leitch, H.G., Nichols, J., and Smith, A. (2019). Defined conditions for propagation and manipulation of mouse embryonic stem cells. Development *146*.
Murakami, K., Gunesdogan, U., Zylicz, J.J., Tang, W.W., Sengupta, R., Kobayashi, T., Kim, S., Butler, R., Dietmann, S., and Surani, M.A. (2016). NANOG alone induces germ cells in primed epiblast in vitro by activation of enhancers. Nature *529*, 403-407.
Najm, F.J., Chenoweth, J.G., Anderson, P.D., Nadeau, J.H., Redline, R.W., McKay, R.D., and Tesar, P.J. (2011). Isolation of epiblast stem cells from preimplantation mouse embryos. Cell Stem Cell *8*, 318-325.
Nakaki, F., Hayashi, K., Ohta, H., Kurimoto, K., Yabuta, Y., and Saitou, M. (2013). Induction of mouse germ-cell fate by transcription factors in vitro. Nature *501*, 222-226.

Nakamura, T., Okamoto, I., Sasaki, K., Yabuta, Y., Iwatani, C., Tsuchiya, H., Seita, Y., Nakamura, S., Yamamoto, T., and Saitou, M. (2016). A developmental coordinate of pluripotency among mice, monkeys and humans. Nature *537*, 57-62.
Nakanishi, M., Mitchell, R.R., Benoit, Y.D., Orlando, L., Reid, J.C., Shimada, K., Davidson, K.C., Shapovalova, Z., Collins, T.J., Nagy, A.*, et al.* (2019). Human Pluripotency Is Initiated and Preserved by a Unique Subset of Founder Cells. Cell.
Neagu, A., van Genderen, E., Escudero, I., Verwegen, L., Kurek, D., Lehmann, J., Stel, J., Dirks, R.A.M., van Mierlo, G., Maas, A.*, et al.* (2020). In vitro capture and characterization of embryonic rosette-stage pluripotency between naive and primed states. Nat Cell Biol *22*, 534-545.
Nichols, J., and Smith, A. (2009). Naive and primed pluripotent states. Cell Stem Cell *4*, 487-492.
Nichols, J., and Ying, Q.L. (2006). Derivation and propagation of embryonic stem cells in serum- and feeder-free culture. Methods Mol Biol *329*, 91-98.
Niswander, L., and Martin, G.R. (1992). Fgf-4 expression during gastrulation, myogenesis, limb and tooth development in the mouse. Development *114*, 755-768.
O'Leary, T., Heindryckx, B., Lierman, S., van Bruggen, D., Goeman, J.J., Vandewoestyne, M., Deforce, D., de Sousa Lopes, S.M., and De Sutter, P. (2012). Tracking the progression of the human inner cell mass during embryonic stem cell derivation. Nat Biotechnol *30*, 278-282.
Ohinata, Y., Ohta, H., Shigeta, M., Yamanaka, K., Wakayama, T., and Saitou, M. (2009). A signaling principle for the specification of the germ cell lineage in mice. Cell *137*, 571-584.
Ohinata, Y., Payer, B., O'Carroll, D., Ancelin, K., Ono, Y., Sano, M., Barton, S.C., Obukhanych, T., Nussenzweig, M., Tarakhovsky, A.*, et al.* (2005). Blimp1 is a critical determinant of the germ cell lineage in mice. Nature *436*, 207-213.
Ohtsuka, S., Nishikawa-Torikai, S., and Niwa, H. (2012). E-cadherin promotes incorporation of mouse epiblast stem cells into normal development. PLoS One *7*, e45220.
Osorno, R., Tsakiridis, A., Wong, F., Cambray, N., Economou, C., Wilkie, R., Blin, G., Scotting, P.J., Chambers, I., and Wilson, V. (2012). The developmental dismantling of pluripotency is reversed by ectopic Oct4 expression. Development *139*, 2288-2298.
Osteil, P., Studdert, J.B., Goh, H.N., Wilkie, E.E., Fan, X., Khoo, P.-L., Peng, G., Salehin, N., Knowles, H., Han, J.-D.J.*, et al.* (2019). Dynamics of Wnt activity on the acquisition of ectoderm potency in epiblast stem cells. Development *146*, dev172858.
Peng, G., Suo, S., Chen, J., Chen, W., Liu, C., Yu, F., Wang, R., Chen, S., Sun, N., Cui, G.*, et al.* (2016). Spatial Transcriptome for the Molecular Annotation of Lineage Fates and Cell Identity in Mid-gastrula Mouse Embryo. Dev Cell *36*, 681-697.
Peng, G., Suo, S., Cui, G., Yu, F., Wang, R., Chen, J., Chen, S., Liu, Z., Chen, G., Qian, Y.*, et al.* (2019). Molecular architecture of lineage allocation and tissue organization in early mouse embryo. Nature *572*, 528-532.
Picelli, S., Faridani, O.R., Bjorklund, A.K., Winberg, G., Sagasser, S., and Sandberg, R. (2014). Full-length RNA-seq from single cells using Smart-seq2. Nat Protoc *9*, 171-181.
Rathjen, J., Lake, J.A., Bettess, M.D., Washington, J.M., Chapman, G., and Rathjen, P.D. (1999). Formation of a primitive ectoderm like cell population, EPL cells, from ES cells in response to biologically derived factors. J Cell Sci *112*, 601-612.
Robertson, E.J. (2014). Dose-dependent Nodal/Smad signals pattern the early mouse embryo. Semin Cell Dev Biol *32*, 73-79.
Rossant, J. (2015). Mouse and human blastocyst-derived stem cells: vive les differences. Development *142*, 9-12.
Rossant, J., and Tam, P.P.L. (2017). New Insights into Early Human Development: Lessons for Stem Cell Derivation and Differentiation. Cell Stem Cell *20*, 18-28.
Rostovskaya, M., Stirparo, G.G., and Smith, A. (2019). Capacitation of human naïve pluripotent stem cells for multi-lineage differentiation. Development *146*, dev172916.
Sasaki, K., Yokobayashi, S., Nakamura, T., Okamoto, I., Yabuta, Y., Kurimoto, K., Ohta, H., Moritoki, Y., Iwatani, C., Tsuchiya, H.*, et al.* (2015). Robust In Vitro Induction of Human Germ Cell Fate from Pluripotent Stem Cells. Cell Stem Cell *17*, 178-194.

Shiura, H., and Abe, K. (2019). Xist/Tsix expression dynamics during mouse peri-implantation development revealed by whole-mount 3D RNA-FISH. Scientific reports *9*.
Smith, A. (2017). Formative pluripotency: the executive phase in a developmental continuum. Development *144*, 365-373.
Smith, A.G., Heath, J.K., Donaldson, D.D., Wong, G.G., Moreau, J., Stahl, M., and Rogers, D. (1988). Inhibition of pluripotential embryonic stem cell differentiation by purified polypeptides. Nature *336*, 688-690.
Solter, D., and Knowles, B. (1975). Immunosurgery of mouse blastocyst. PNAS *72*, 5099-5102.
Sousa, E.J., Stuart, H.T., Bates, L.E., Ghorbani, M., Nichols, J., Dietmann, S., and Silva, J.C.R. (2018). Exit from Naive Pluripotency Induces a Transient X Chromosome Inactivation-like State in Males. Cell Stem Cell *22*, 919-928 e916.
Stavridis, M.P., Collins, B.J., and Storey, K.G. (2010). Retinoic acid orchestrates fibroblast growth factor signalling to drive embryonic stem cell differentiation. Development *137*, 881-890.
Stavridis, M.P., Lunn, J.S., Collins, B.J., and Storey, K.G. (2007). A discrete period of FGF-induced Erk1/2 signalling is required for vertebrate neural specification. Development *134*, 2889-2894.
Stavridis, M.P., and Smith, A.G. (2003). Neural differentiation of mouse embryonic stem cells. Biochem Soc Trans *31*, 45-49.
Strawbridge, S.E., Blanchard, G.B., Smith, A., Kugler, H., and Martello, G. (2020). Embryonic stem cells commit to differentiation by symmetric divisions following a variable lag period. bioRxiv, 2020.2006.2017.157578.
Sun, X., Meyers, E.N., Lewandoski, M., and Martin, G.R. (1999). Targeted disruption of Fgf8 causes failure of cell migration in the gastrulating mouse embryo. Genes & Development *13*, 1834-1846.
Takashima, Y., Guo, G., Loos, R., Nichols, J., Ficz, G., Krueger, F., Oxley, D., Santos, F., Clarke, J., Mansfield, W.*, et al.* (2014). Resetting Transcription Factor Control Circuitry toward Ground-State Pluripotency in Human. Cell *158*, 1254-1269.
Takenaga, M., Fukumoto, M., and Hori, Y. (2007). Regulated Nodal signaling promotes differentiation of the definitive endoderm and mesoderm from ES cells. J Cell Sci *120*, 2078-2090.
Tesar, P.J., Chenoweth, J.G., Brook, F.A., Davies, T.J., Evans, E.P., Mack, D.L., Gardner, R.L., and McKay, R.D. (2007). New cell lines from mouse epiblast share defining features with human embryonic stem cells. Nature *448*, 196-199.
Theunissen, T.W., Friedli, M., He, Y., Planet, E., O'Neil, R.C., Markoulaki, S., Pontis, J., Wang, H., Iouranova, A., Imbeault, M.*, et al.* (2016). Molecular Criteria for Defining the Naive Human Pluripotent State. Cell Stem Cell *19*, 502-515.
Tsakiridis, A., Huang, Y., Blin, G., Skylaki, S., Wymeersch, F., Osorno, R., Economou, C., Karagianni, E., Zhao, S., Lowell, S.*, et al.* (2014). Distinct Wnt-driven primitive streak-like populations reflect in vivo lineage precursors. Development *141*, 1209-1221.
Varlet, I., Collignon, J., and Robertson, E.J. (1997). nodal expression in the primitive endoderm is required for specification of the anterior axis during mouse gastrulation. Development *124*, 1033-1044.
Watanabe, K., Ueno, M., Kamiya, D., Nishiyama, A., Matsumura, M., Wataya, T., Takahashi, J.B., Nishikawa, S., Nishikawa, S., Muguruma, K.*, et al.* (2007). A ROCK inhibitor permits survival of dissociated human embryonic stem cells. Nat Biotechnol *25*, 681-686.
Williams, R.L., Hilton, D.J., Pease, S., Willson, T.A., Stewart, C.L., Gearing, D.P., Wagner, E.F., Metcalf, D., Nicola, N.A., and Gough, N.M. (1988). Myeloid leukaemia inhibitory factor maintains the developmental potential of embryonic stem cells. Nature *336*, 684-687.
Winnier, G., Blessing, M., Labosky, P.A., and Hogan, B.L. (1995). Bone morphogenetic protein-4 is required for mesoderm formation and patterning in the mouse. Genes Dev *9*, 2105-2116.
Xiang, L., Yin, Y., Zheng, Y., Ma, Y., Li, Y., Zhao, Z., Guo, J., Ai, Z., Niu, Y., Duan, K.*, et al.* (2019). A developmental landscape of 3D-cultured human pre-gastrulation embryos. Nature.

Yang, S.H., Kalkan, T., Morissroe, C., Marks, H., Stunnenberg, H., Smith, A., and Sharrocks, A.D. (2014). Otx2 and Oct4 Drive Early Enhancer Activation during Embryonic Stem Cell Transition from Naive Pluripotency. Cell Rep *7*, 1968-1981.
Zerbino, D.R., Johnson, N., Juettemann, T., Wilder, S.P., and Flicek, P. (2014). WiggleTools: parallel processing of large collections of genome-wide datasets for visualization and statistical analysis. Bioinformatics *30*, 1008-1009.
Zhang, Z., Verheyden, J.M., Hassell, J.A., and Sun, X. (2009). FGF-regulated Etv genes are essential for repressing Shh expression in mouse limb buds. Dev Cell *16*, 607-613.
Zylicz, J.J., Dietmann, S., Gunesdogan, U., Hackett, J.A., Cougot, D., Lee, C., and Surani, M.A. (2015). Chromatin dynamics and the role of G9a in gene regulation and enhancer silencing during early mouse development. Elife *4*.

Fig1

A

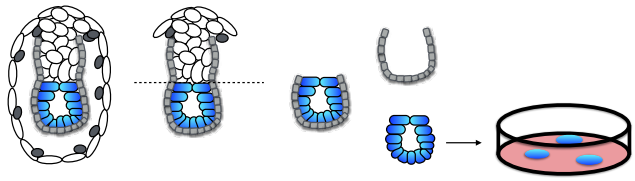

B

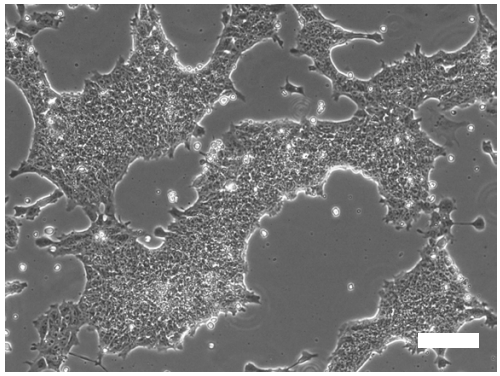

C

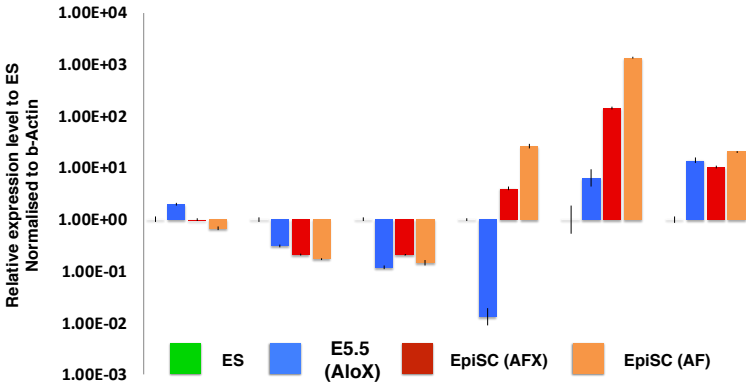

D

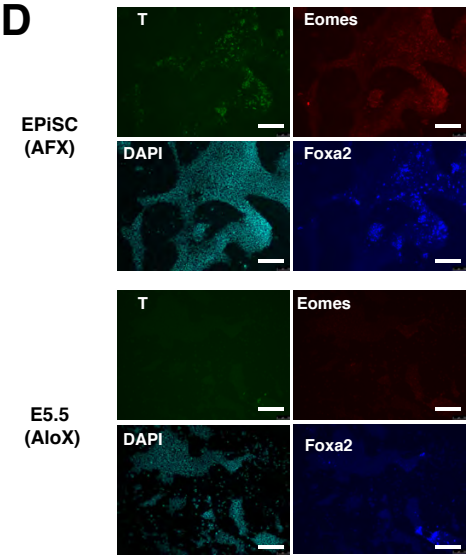

E

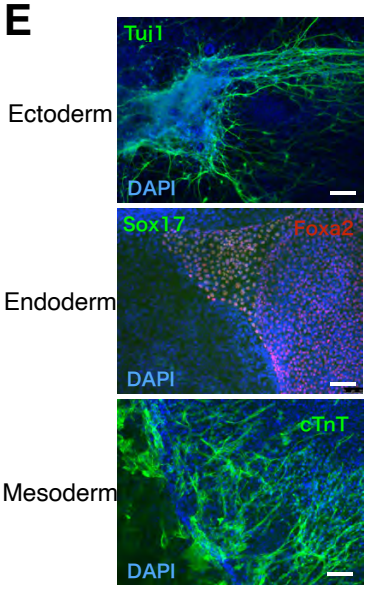

F

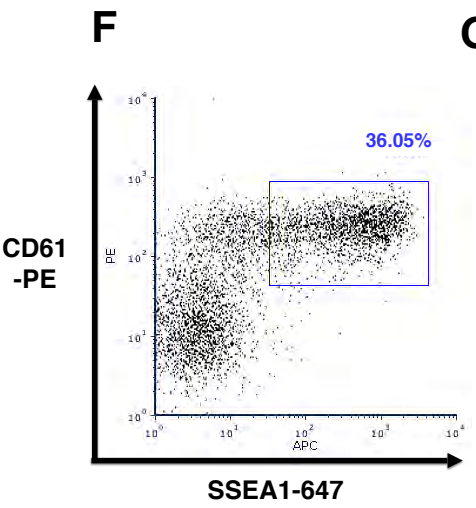

G

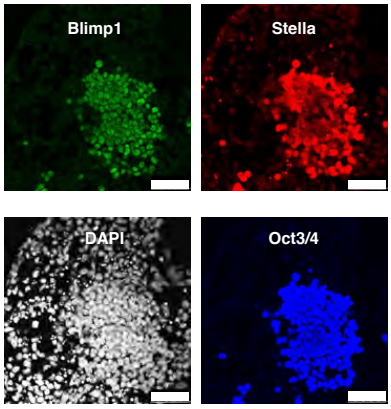

Fig. 2

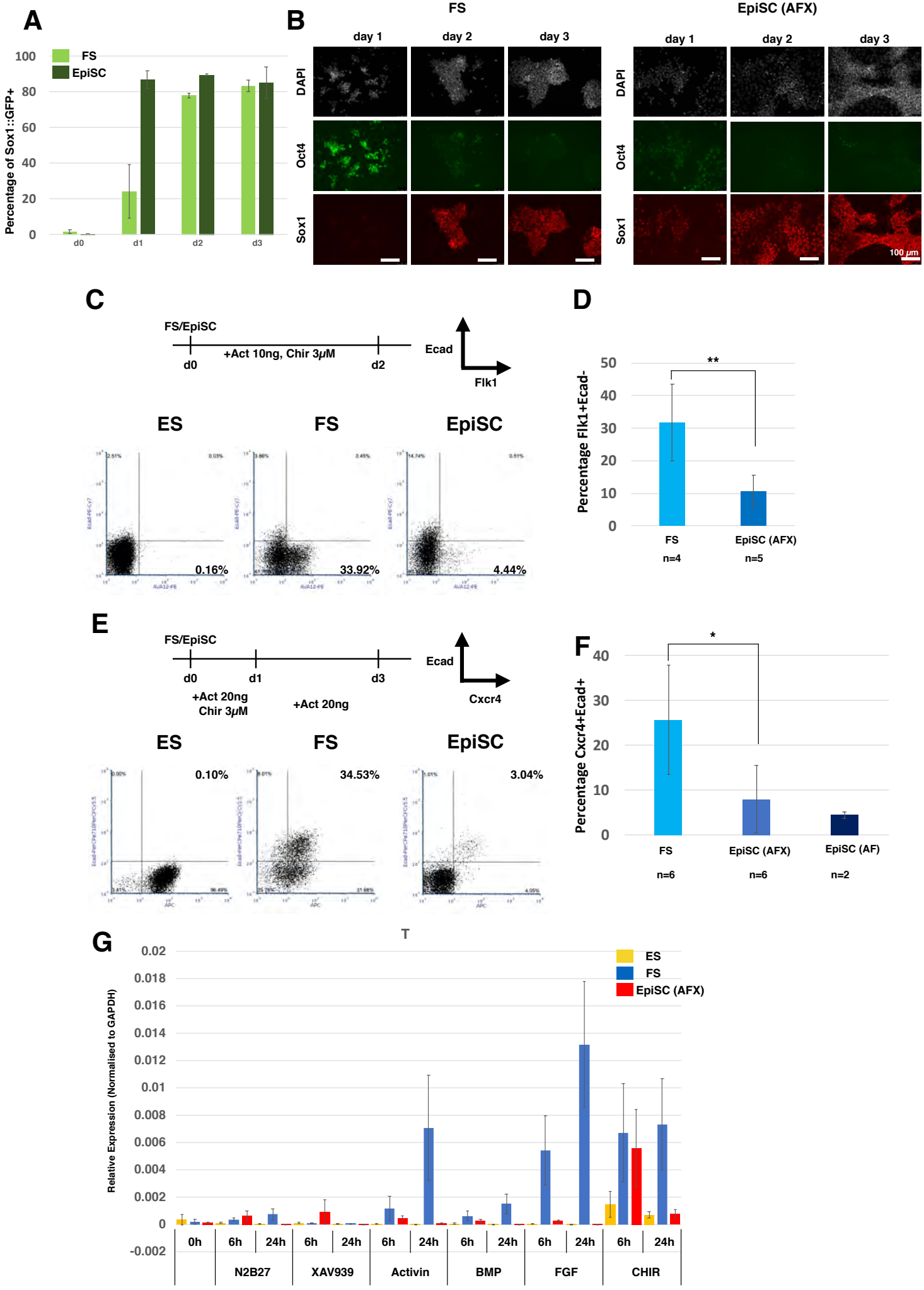
A
FS
EpiSC
Percentage of Sox1::GFP+
100
80
60
40
20
0
d0
d1
d2
d3
B
FS
EpiSC (AFX)
day 1
day 2
day 3
DAPI
Oct4
Sox1
100 μm
C
FS/EpiSC
+Act 10ng, Chir 3μM
d0
d2
Ecad
Flk1
ES
FS
EpiSC
0.16%
33.92%
4.44%
D
Percentage Flk1+Ecad-
50
40
30
20
10
0
**
FS
n=4
EpiSC (AFX)
n=5
E
FS/EpiSC
d0
d1
d3
+Act 20ng
Chir 3μM
+Act 20ng
Ecad
Cxcr4
ES
FS
EpiSC
0.10%
34.53%
3.04%
F
Percentage Cxcr4+Ecad+
40
30
20
10
0
*
FS
n=6
EpiSC (AFX)
n=6
EpiSC (AF)
n=2
G
T
Relative Expression (Normalised to GAPDH)
0.02
0.018
0.016
0.014
0.012
0.01
0.008
0.006
0.004
0.002
0
-0.002
ES
FS
EpiSC (AFX)
0h
6h
24h
N2B27
XAV939
Activin
BMP
FGF
CHIR

Fig. 3

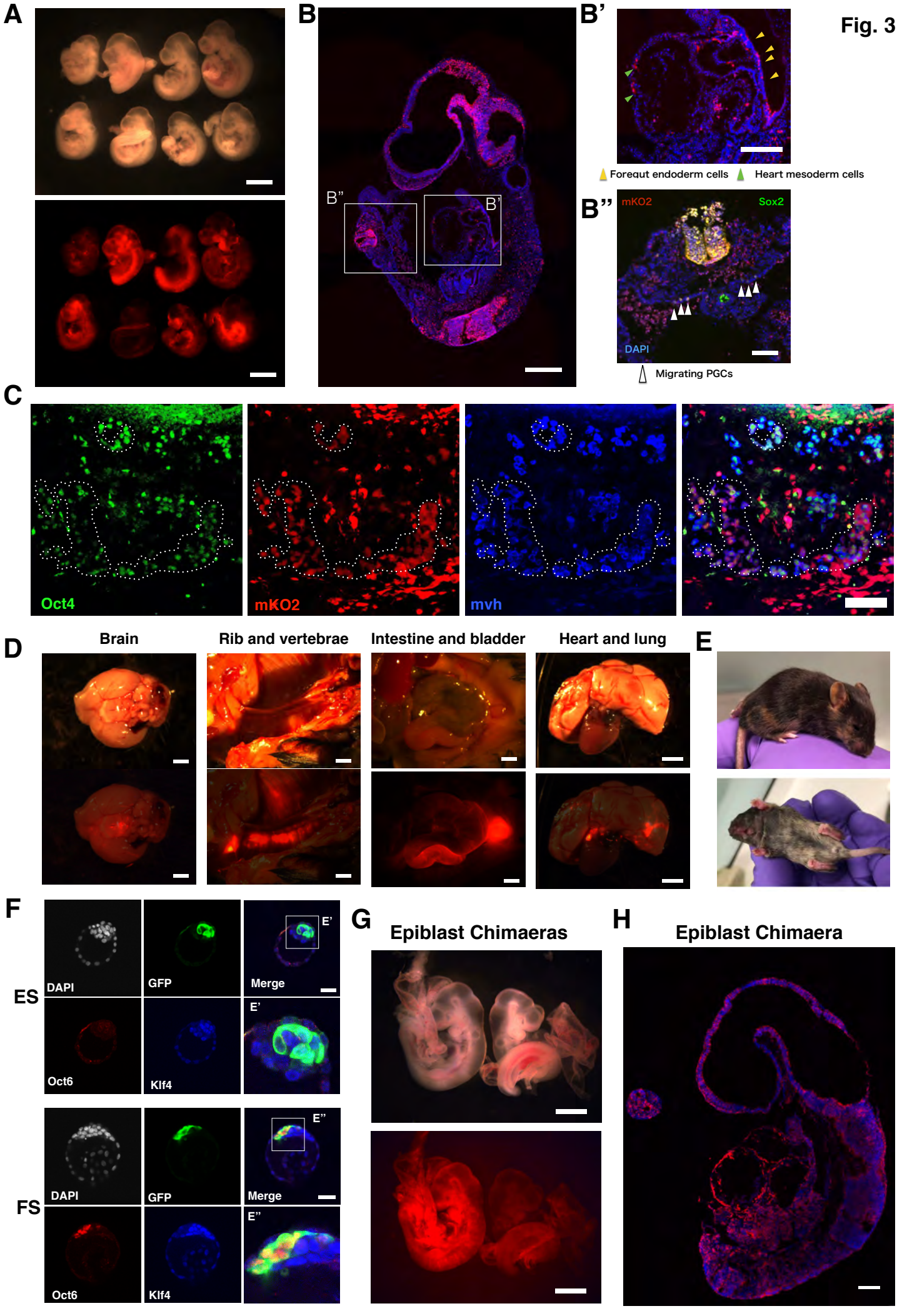
A
B
B'
B''
Foregut endoderm cells
Heart mesoderm cells
mKO2
Sox2
DAPI
Migrating PGCs
C
Oct4
mKO2
mvh
D
Brain
Rib and vertebrae
Intestine and bladder
Heart and lung
E
F
ES
FS
DAPI
GFP
Merge
Oct6
Klf4
G
Epiblast Chimaeras
H
Epiblast Chimaera

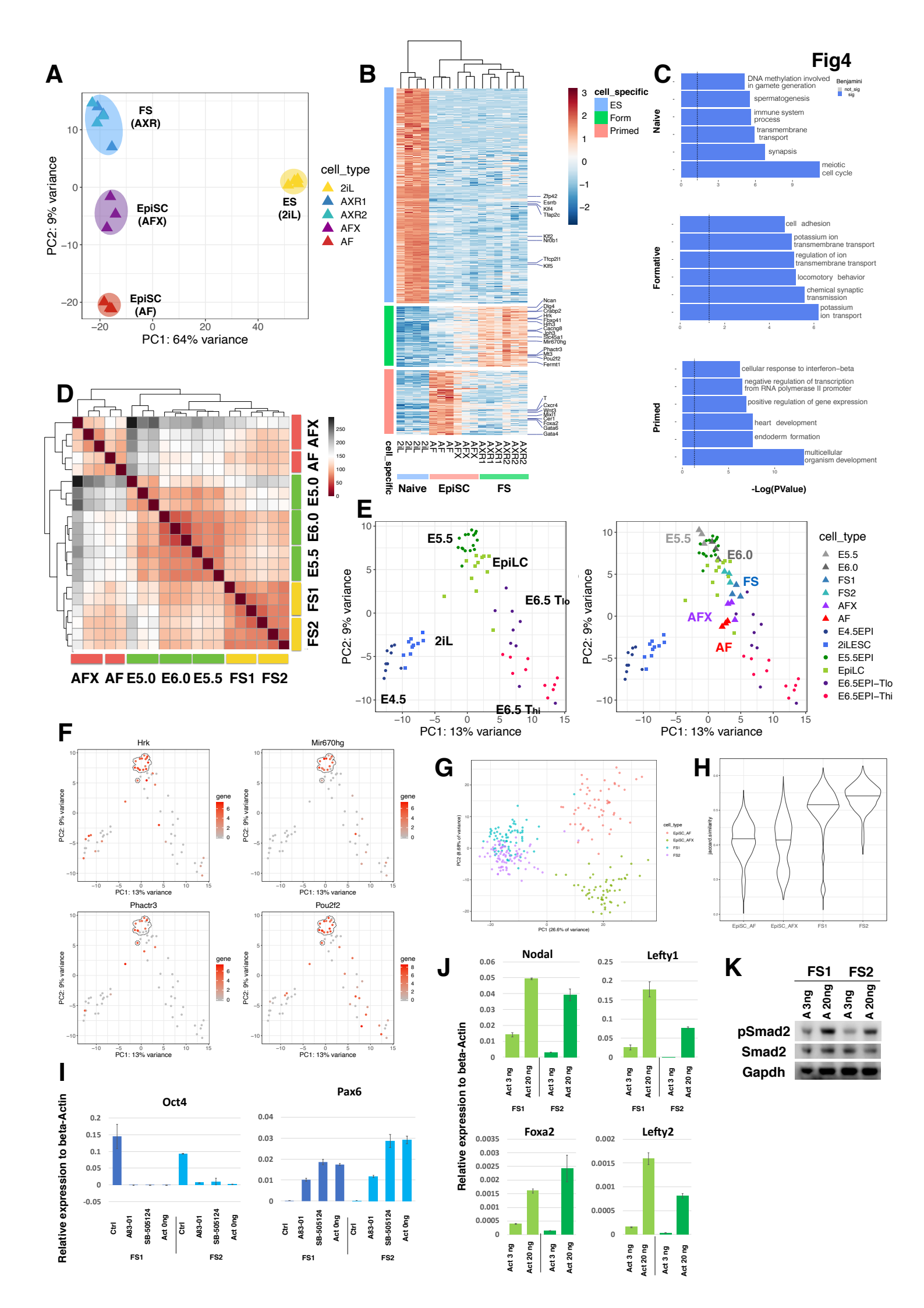
Fig4
A
FS (AXR)
EpiSC (AFX)
ES (2iL)
EpiSC (AF)
PC2: 9% variance
PC1: 64% variance
cell_type
2iL
AXR1
AXR2
AFX
AF
B
cell_specific
ES
Form
Primed
Naive
EpiSC
FS
C
Naive
DNA methylation involved in gamete generation
spermatogenesis
immune system process
transmembrane transport
synapsis
meiotic cell cycle
Formative
cell adhesion
potassium ion transmembrane transport
regulation of ion transmembrane transport
locomotory behavior
chemical synaptic transmission
potassium ion transport
Primed
cellular response to interferon−beta
negative regulation of transcription from RNA polymerase II promoter
positive regulation of gene expression
heart development
endoderm formation
multicellular organism development
Benjamini
not_sig
sig
-Log(PValue)
D
AFX AF E5.0 E6.0 E5.5 FS1 FS2
E
E5.5
EpiLC
E6.5 Tlo
2iL
E4.5
E6.5 Thi
PC1: 13% variance
PC2: 9% variance
E6.0
FS
AFX
AF
cell_type
E5.5
E6.0
FS1
FS2
AFX
AF
E4.5EPI
2iLESC
E5.5EPI
EpiLC
E6.5EPI−Tlo
E6.5EPI−Thi
F
Hrk
Mir670hg
Phactr3
Pou2f2
gene
G
H
jaccard similarity
EpiSC_AF
EpiSC_AFX
FS1
FS2
I
Oct4
Pax6
Relative expression to beta-Actin
Ctrl
A83-01
SB-505124
Act 0ng
J
Nodal
Lefty1
Foxa2
Lefty2
Act 3 ng
Act 20 ng
K
FS1
FS2
A 3ng
A 20ng
pSmad2
Smad2
Gapdh

Fig. 5

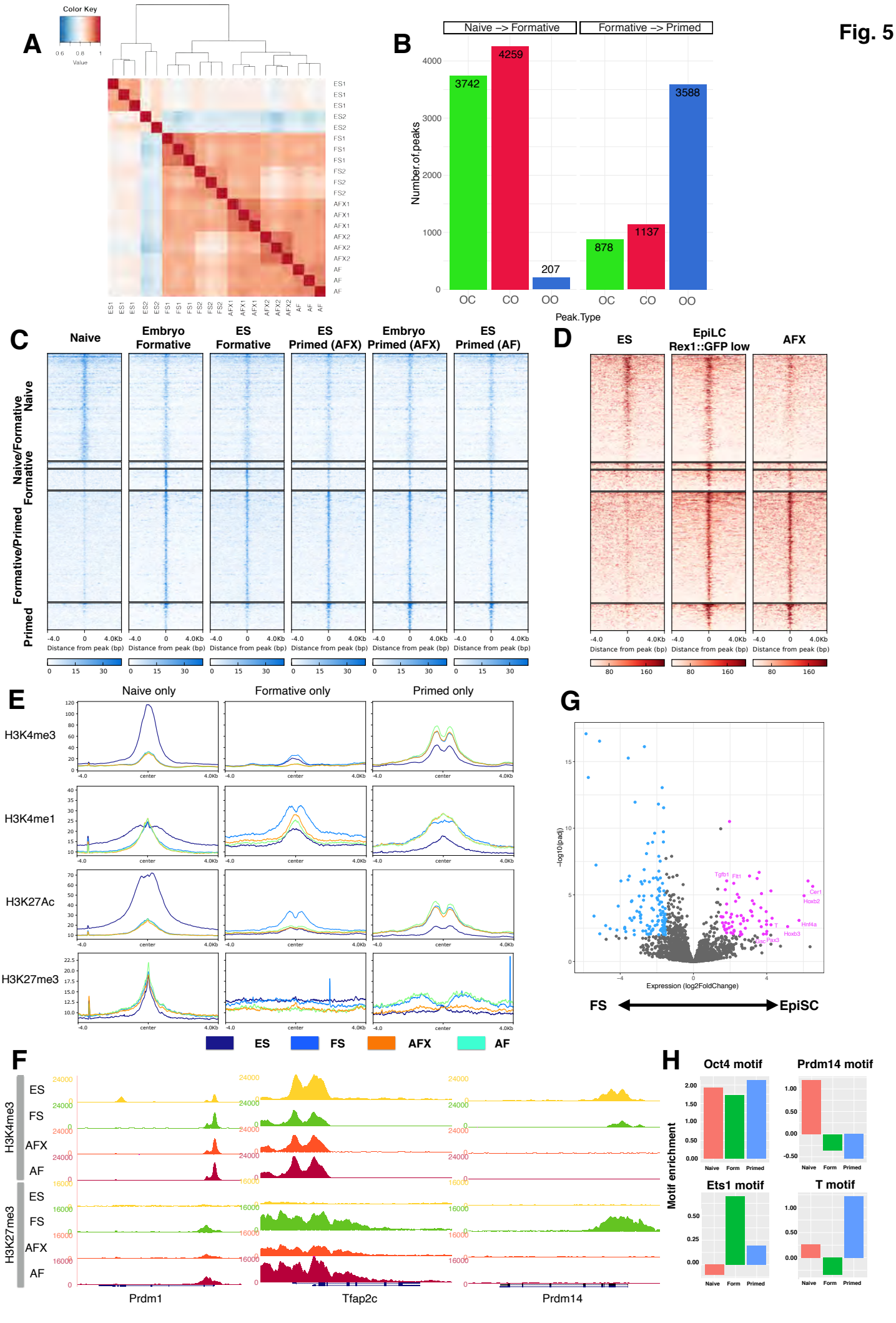
A
Color Key
Value
ES1
ES1
ES1
ES2
ES2
FS1
FS1
FS1
FS2
FS2
FS2
AFX1
AFX1
AFX1
AFX2
AFX2
AFX2
AF
AF
AF
B
Naive –> Formative
Formative –> Primed
Number.of.peaks
4000
3000
2000
1000
0
3742
4259
207
878
1137
3588
OC
CO
OO
OC
CO
OO
Peak.Type
C
Naive
Embryo Formative
ES Formative
ES Primed (AFX)
Embryo Primed (AFX)
ES Primed (AF)
Naive
Naive/Formative
Formative
Formative/Primed
Primed
-4.0
0
4.0Kb
Distance from peak (bp)
0
15
30
D
ES
EpiLC Rex1::GFP low
AFX
80
160
E
Naive only
Formative only
Primed only
H3K4me3
H3K4me1
H3K27Ac
H3K27me3
center
ES
FS
AFX
AF
G
−log10(padj)
Expression (log2FoldChange)
Tgfb1
Flt1
Cer1
Hoxb2
T
Hnf4a
Hoxb3
Foxp3
FS
EpiSC
F
H3K4me3
H3K27me3
ES
FS
AFX
AF
24000
16000
Prdm1
Tfap2c
Prdm14
H
Motif enrichment
Oct4 motif
Prdm14 motif
Ets1 motif
T motif
Naive
Form
Primed

Fig. 6

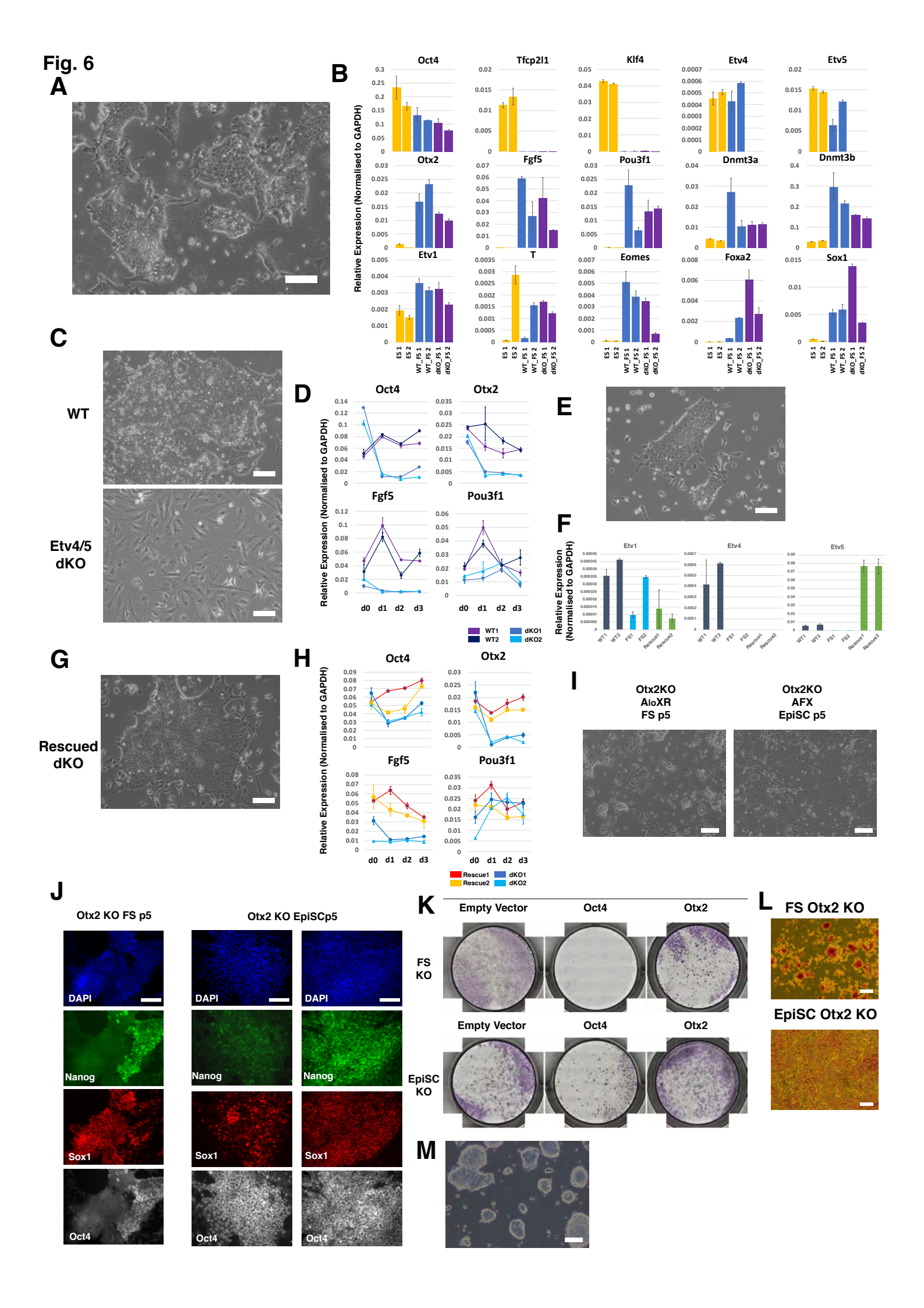
A
B
Oct4
Tfcp2l1
Klf4
Etv4
Etv5
Otx2
Fgf5
Pou3f1
Dnmt3a
Dnmt3b
Etv1
T
Eomes
Foxa2
Sox1
Relative Expression (Normalised to GAPDH)
ES 1
ES 2
WT_FS 1
WT_FS 2
dKO_FS 1
dKO_FS 2
C
WT
Etv4/5 dKO
D
Oct4
Otx2
Fgf5
Pou3f1
Relative Expression (Normalised to GAPDH)
d0 d1 d2 d3
WT1
WT2
dKO1
dKO2
E
F
Etv1
Etv4
Etv5
Relative Expression (Normalised to GAPDH)
WT1
WT2
FS1
FS2
Rescue1
Rescue2
G
Rescued dKO
H
Oct4
Otx2
Fgf5
Pou3f1
Relative Expression (Normalised to GAPDH)
d0 d1 d2 d3
Rescue1
Rescue2
dKO1
dKO2
I
Otx2KO AloXR FS p5
Otx2KO AFX EpiSC p5
J
Otx2 KO FS p5
Otx2 KO EpiSCp5
DAPI
Nanog
Sox1
Oct4
K
Empty Vector
Oct4
Otx2
FS KO
EpiSC KO
L
FS Otx2 KO
EpiSC Otx2 KO
M

Fig. 7

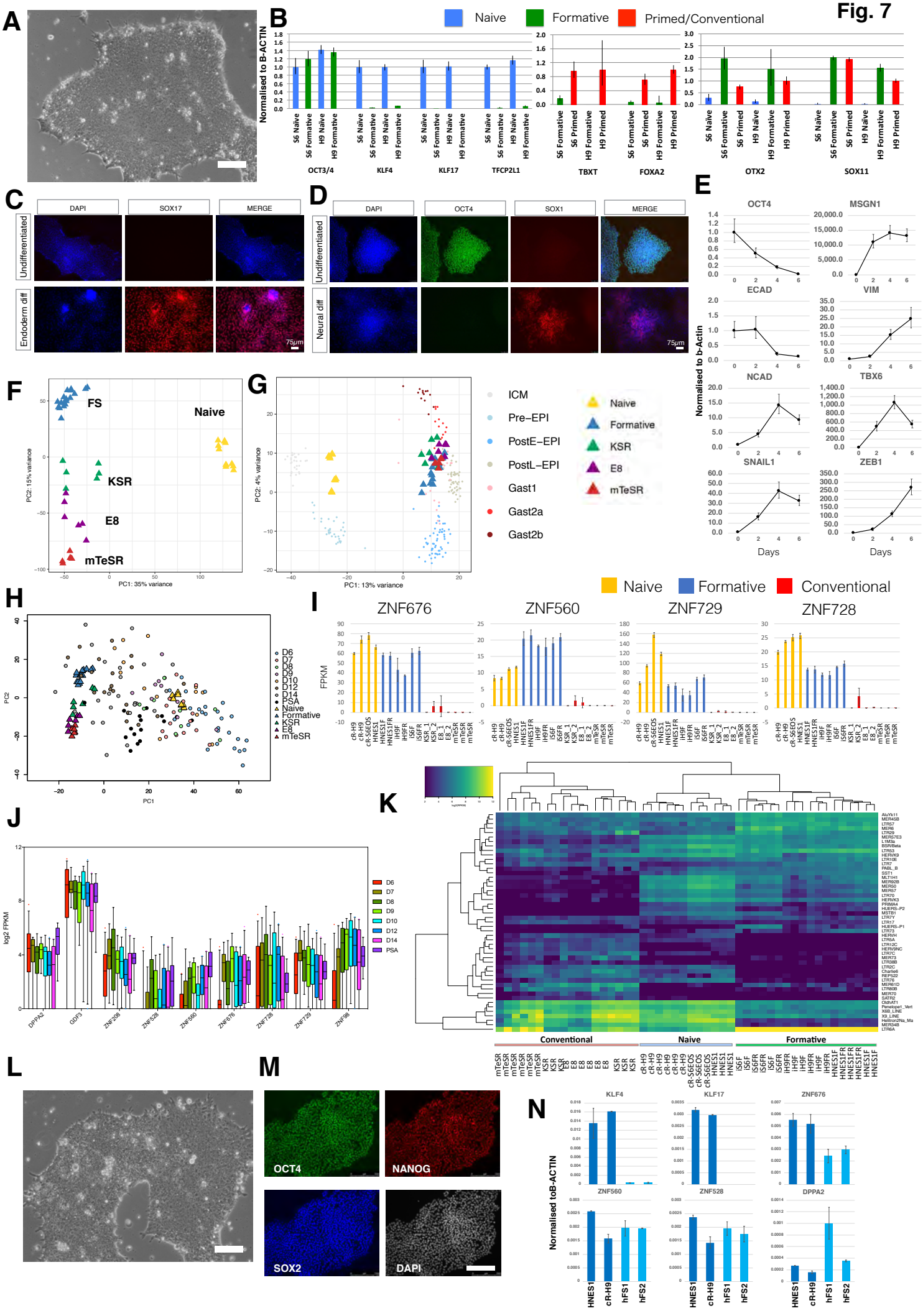
A
B
Naive
Formative
Primed/Conventional
Normalised to B-ACTIN
OCT3/4
KLF4
KLF17
TFCP2L1
TBXT
FOXA2
OTX2
SOX11
C
DAPI
SOX17
MERGE
Undifferentiated
Endoderm diff
75μm
D
DAPI
OCT4
SOX1
MERGE
Undifferentiated
Neural diff
75μm
E
OCT4
MSGN1
ECAD
VIM
NCAD
TBX6
SNAIL1
ZEB1
Normalised to b-Actin
Days
F
FS
Naive
KSR
E8
mTeSR
PC1: 35% variance
PC2: 15% variance
G
ICM
Pre−EPI
PostE−EPI
PostL−EPI
Gast1
Gast2a
Gast2b
Naive
Formative
KSR
E8
mTeSR
PC1: 13% variance
PC2: 4% variance
H
D6
D7
D8
D9
D10
D12
D14
PSA
Naive
Formative
KSR
E8
mTeSR
PC1
PC2
I
Naive
Formative
Conventional
ZNF676
ZNF560
ZNF729
ZNF728
FPKM
J
log2 FPKM
D6
D7
D8
D9
D10
D12
D14
PSA
DPPA2
GDF3
ZNF208
ZNF528
ZNF560
ZNF676
ZNF728
ZNF729
ZNF98
K
Conventional
Naive
Formative
L
M
OCT4
NANOG
SOX2
DAPI
N
KLF4
KLF17
ZNF676
ZNF560
ZNF528
DPPA2
Normalised toB-ACTIN
HNES1
cR-H9
hFS1
hFS2

Figure S1 (Related to Figure 1)

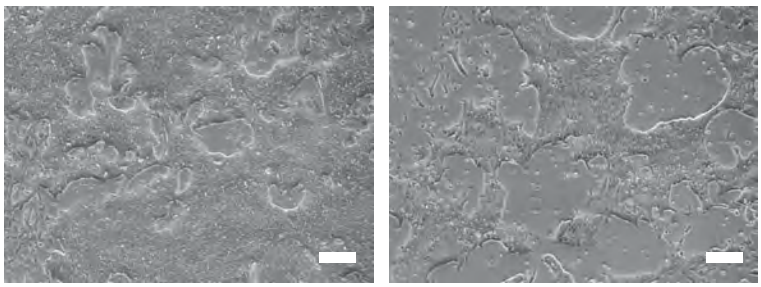

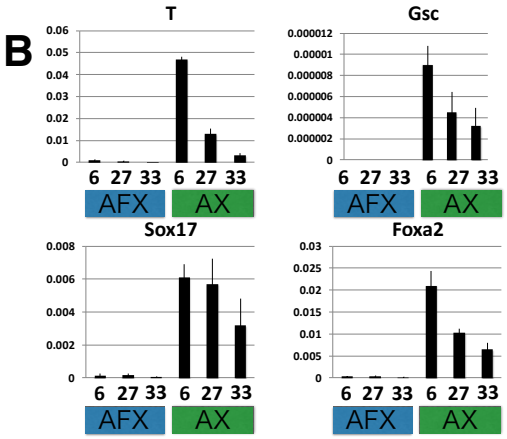

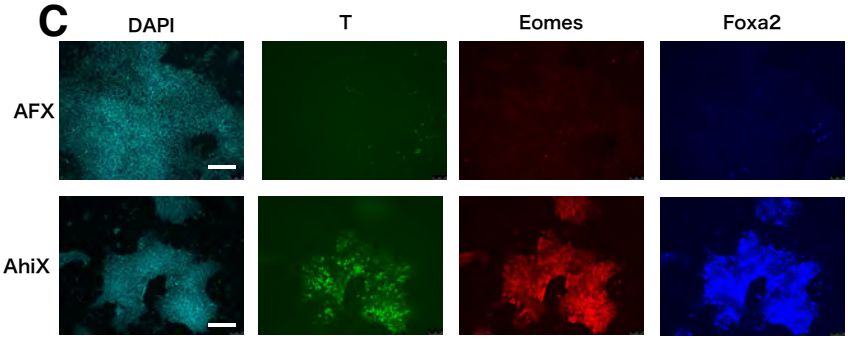

D

Concentration of activin	No of E5.5 embryos	No of established lines (> p10)	Success rate
1ng	8	0	0.0%
1.5ng	8	1	12.5%
2ng	11	3	27.3%
2.5ng	4	0	0.0%
3ng	11	4	36.4%

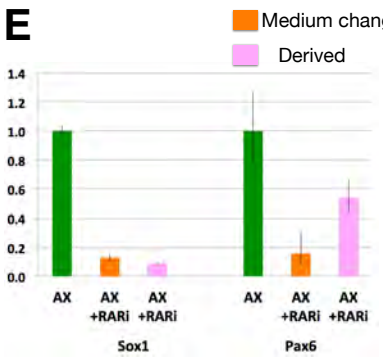

F

	Number of E5.5 embryos	Lines established	Efficiency
AloX	8	4	50%
AloX +RARi	4	4	100%

G

Line	Percentage of diploid (=40) cells	Passage number
5a6	75.0 % (24/32)	19
NBRA3.2	87.1 % (27/31)	22
5ar1	64.0 % (16/25)	21
5ar2	83.3% (20/24)	26

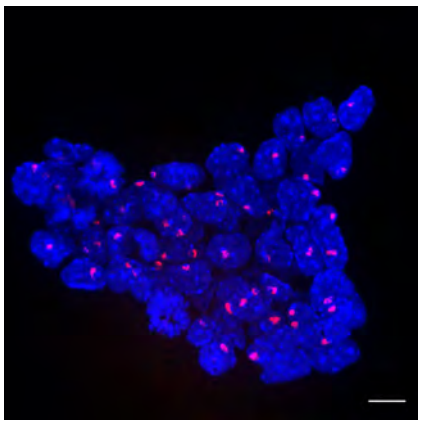

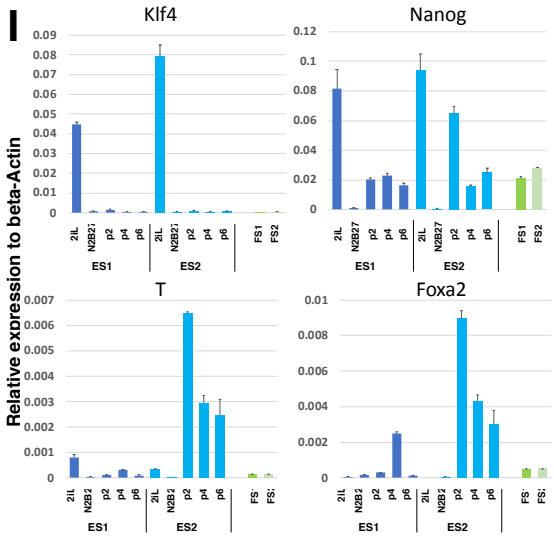

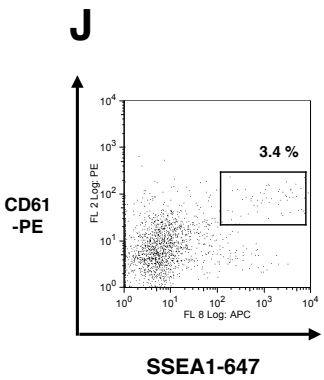

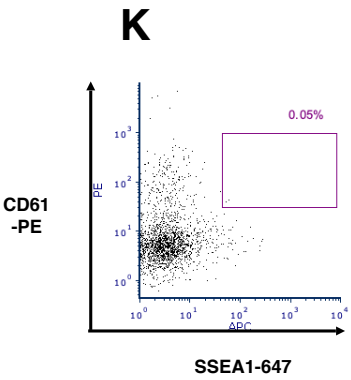

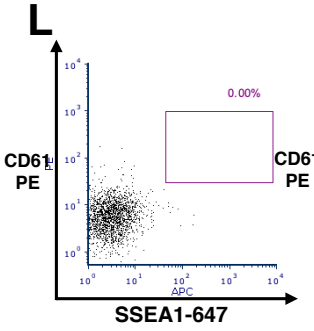

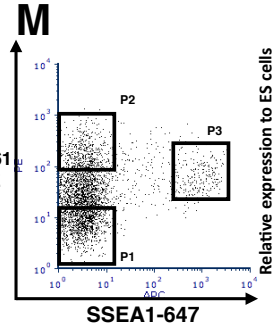

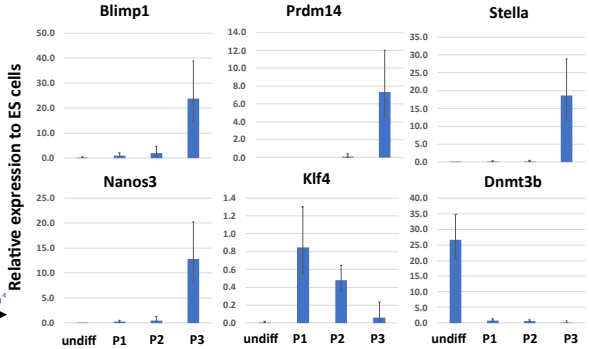

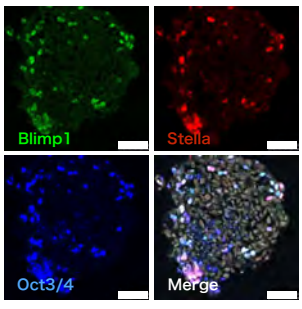

Figure S2 (Related to Figure 2)

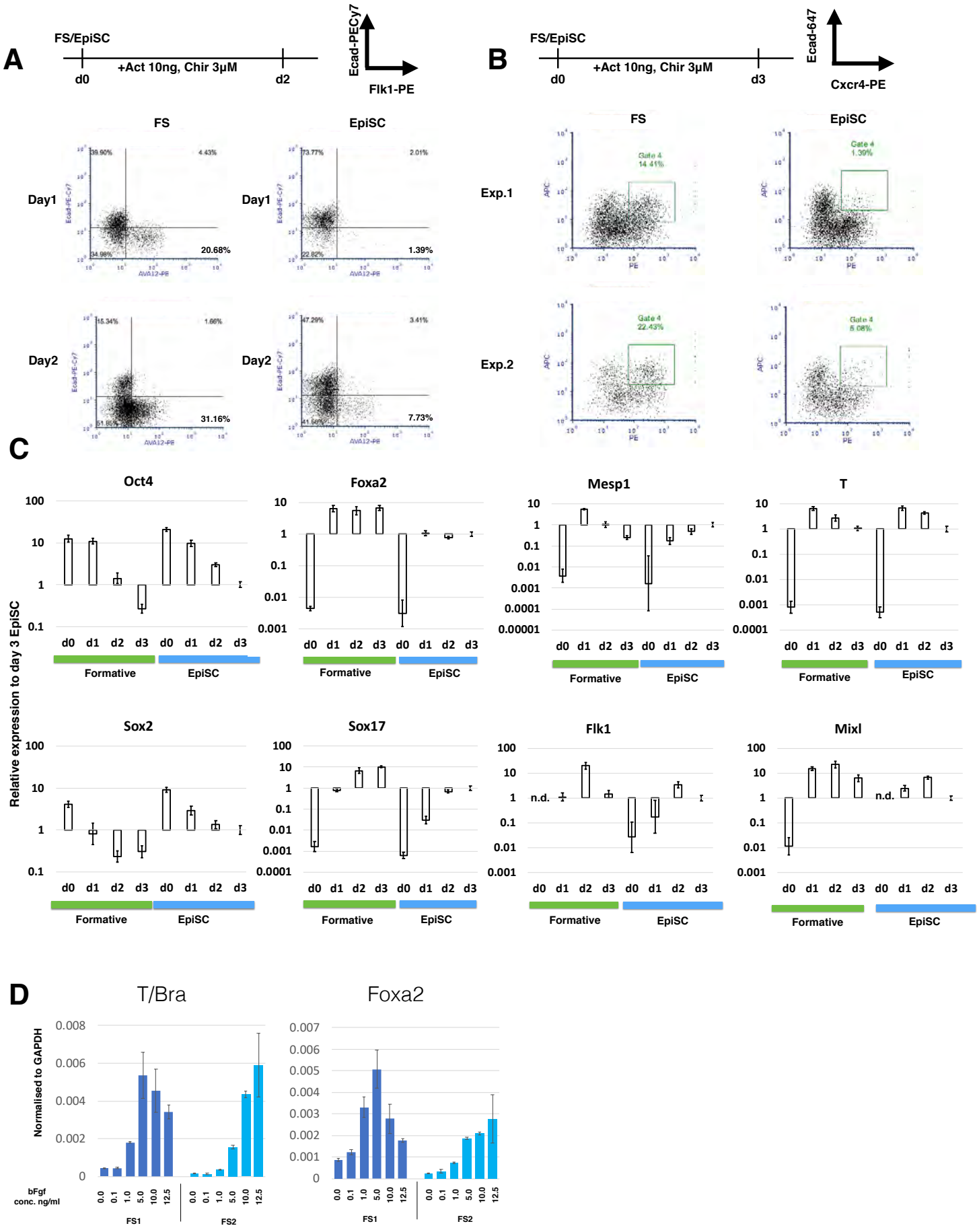

Figure S3 (Related to Figure 3)

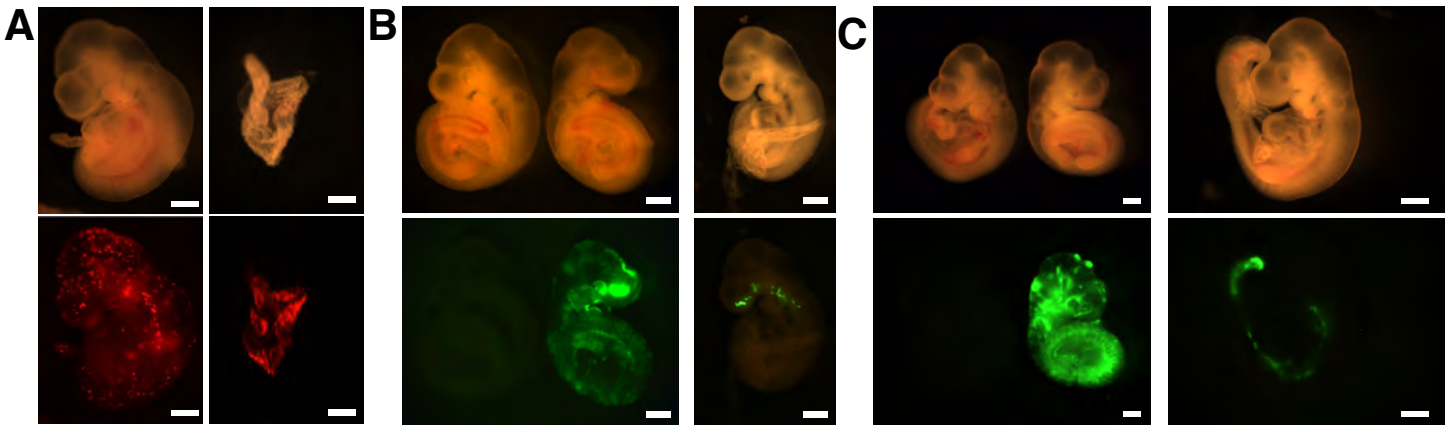

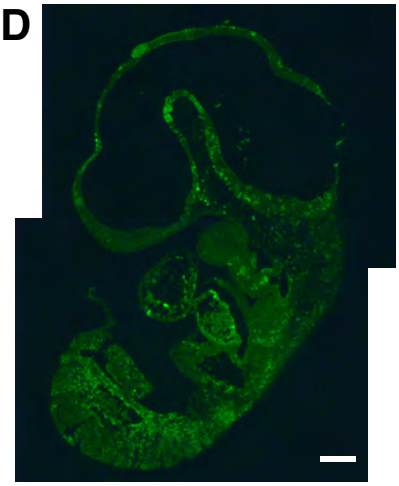

E

Line	Embryos recovered	Widespread Contribution	Localised contribution	Yolk sac contribution	Chimaera rate
NBRA3.2	48	8	11	1*	39.6%
5a6	20	1	2	1	15.0%
5ar1	17	1	3	Not Investigated	23.5%

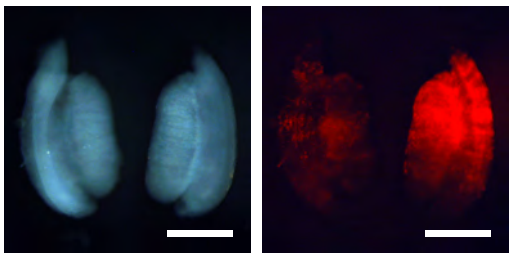

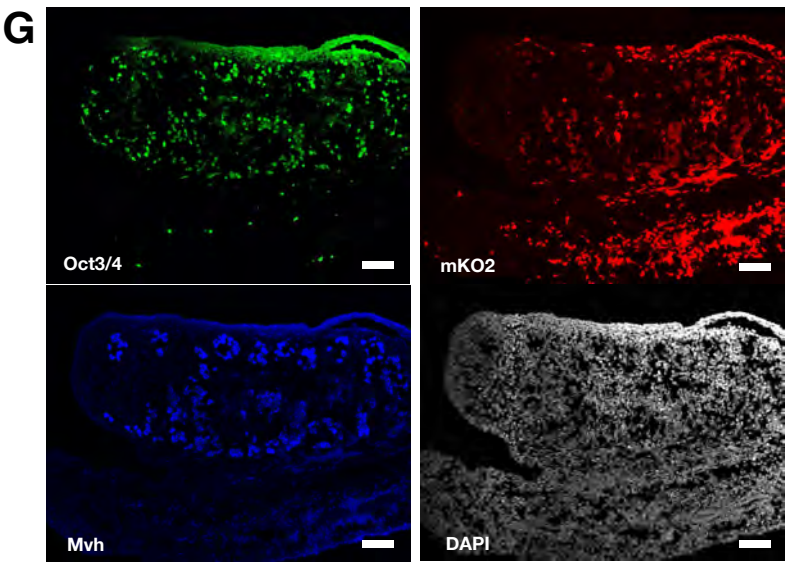

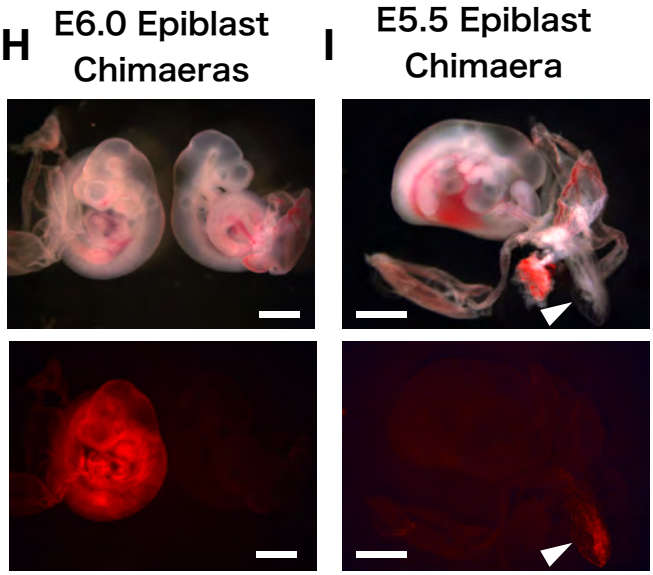

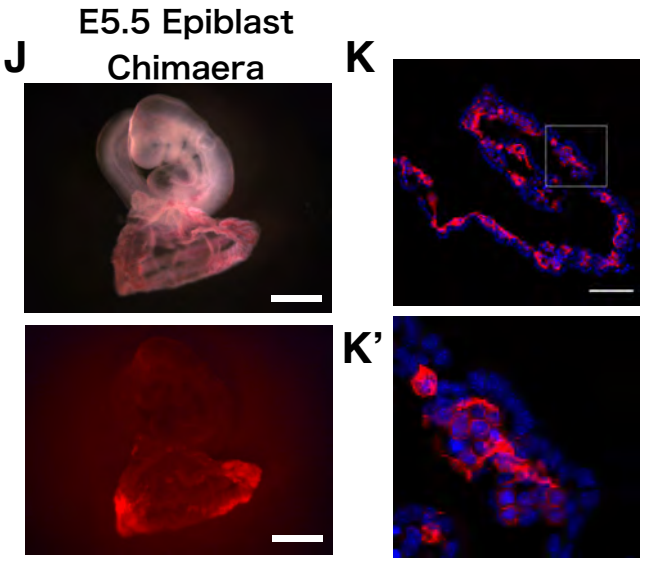

L

Donor stage	Embryos recovered	Widespread Contribution	Localised contribution	contribution yolk sac and/or amnion	Chimaera rate
E5.5	44	2	5	7	16.0%
E6.0	47	1	3	4	8.5%
E6.5	29	0	0	0	0.0%

Figure S4 (Related to Figure 4)

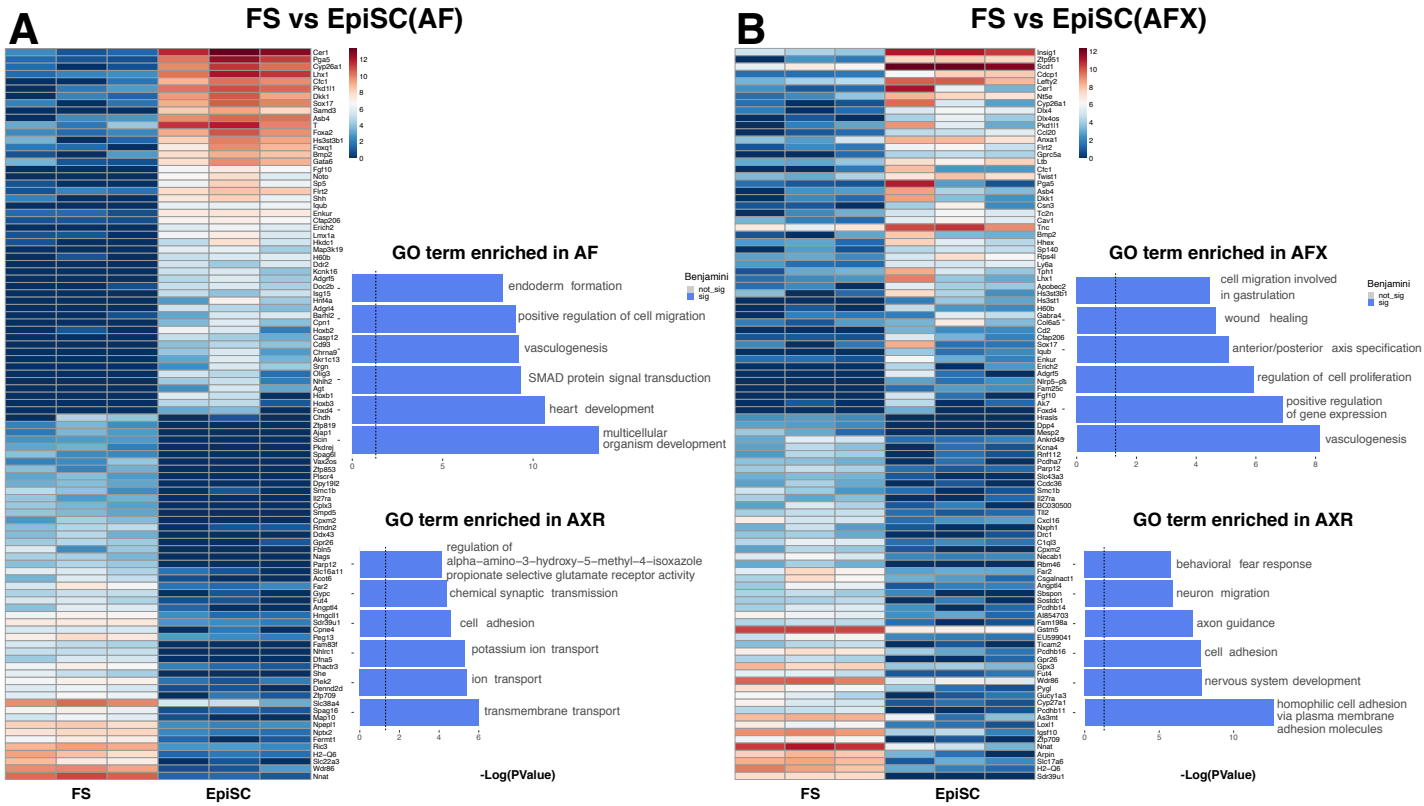

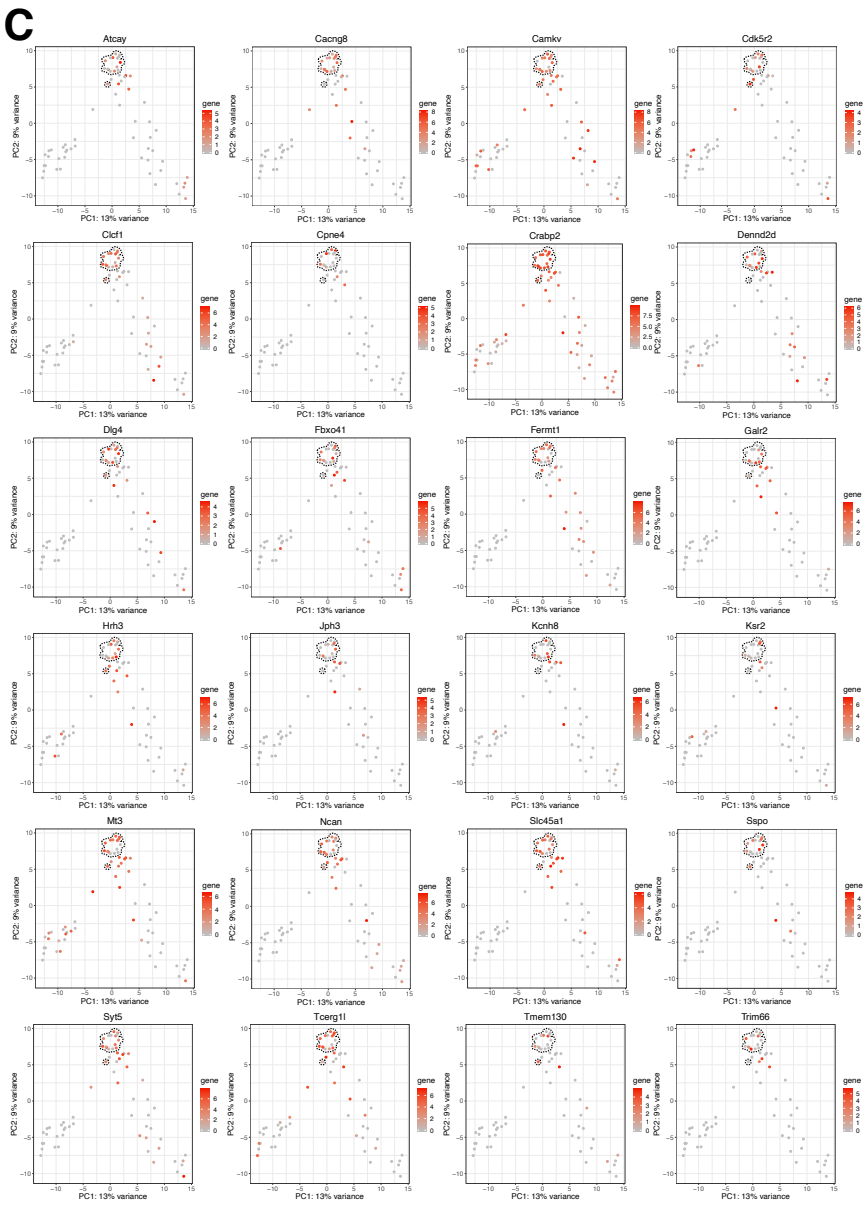

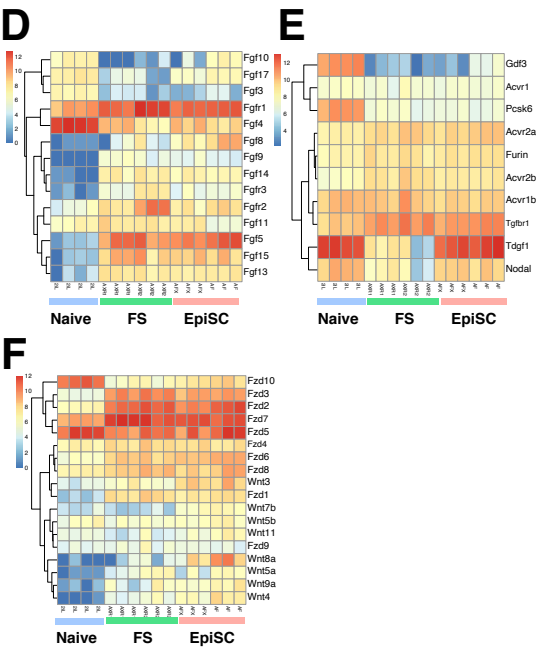

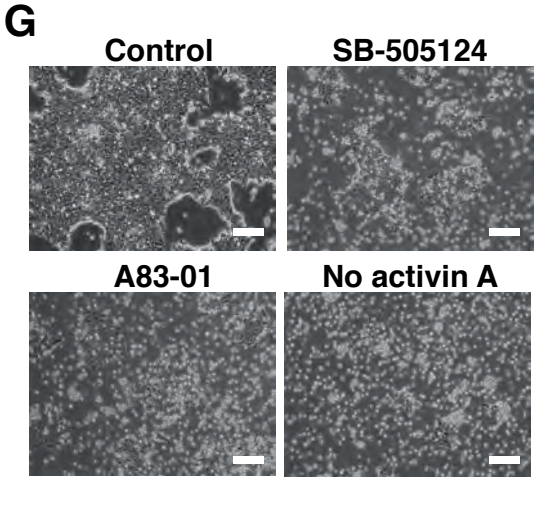

Figure S5 (Related to Figure 5)

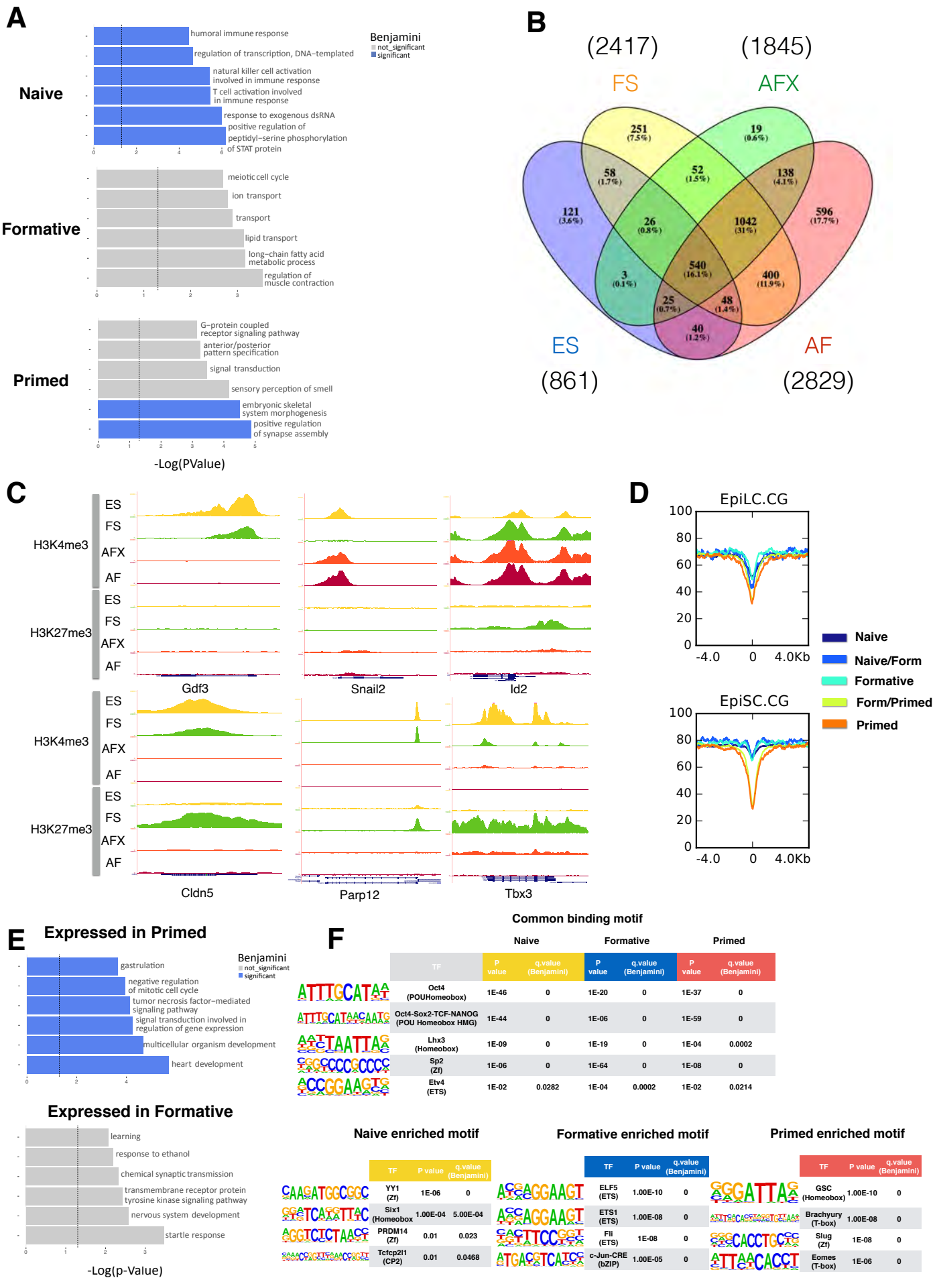

Figure S6 (Related to Figure 6)

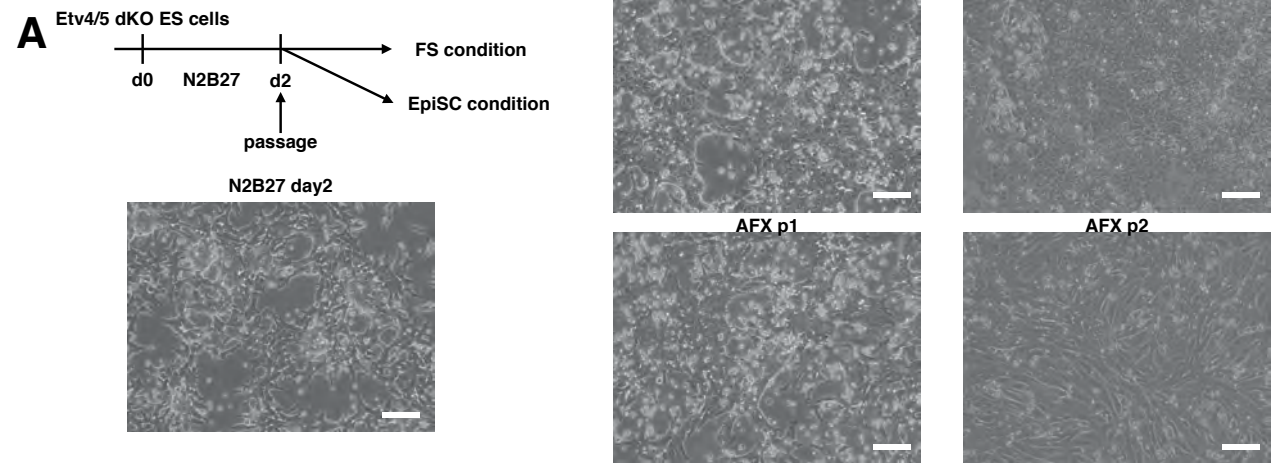

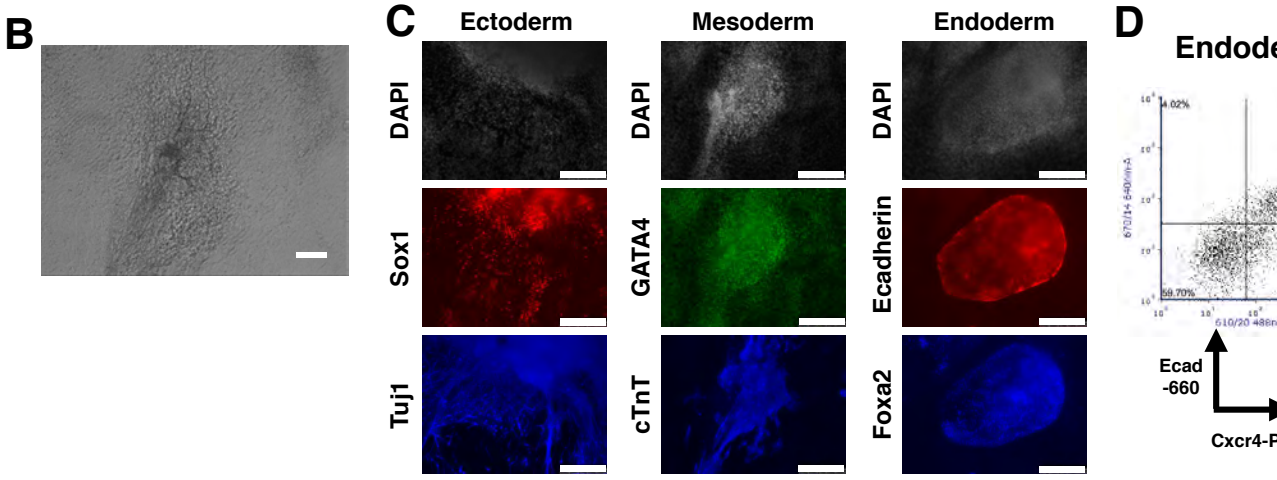

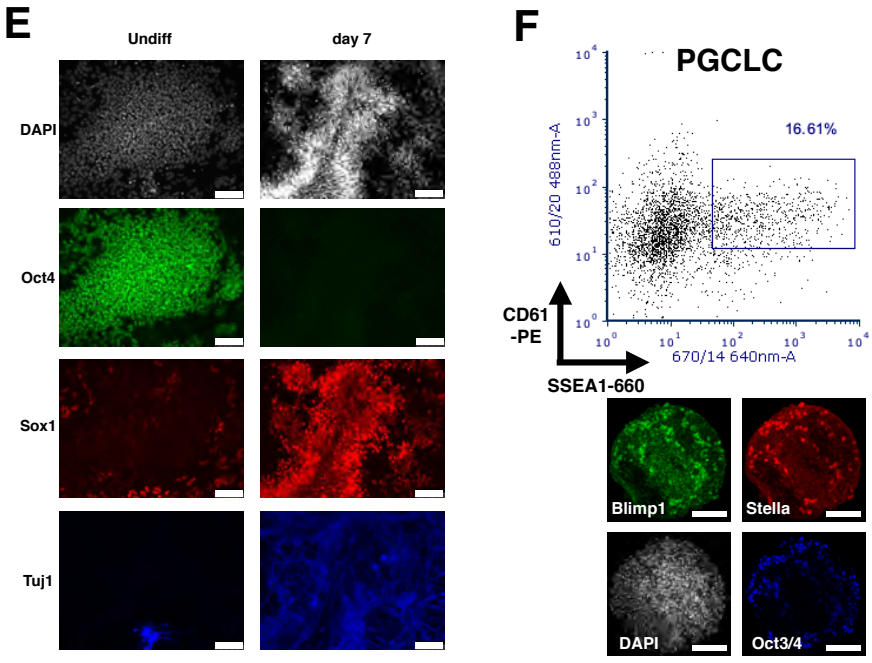

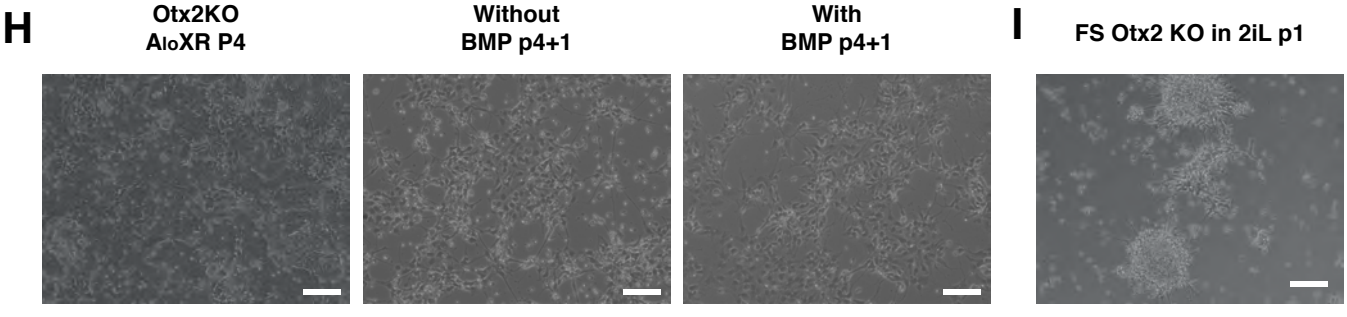

Figure S7 (Related to Figure 7)

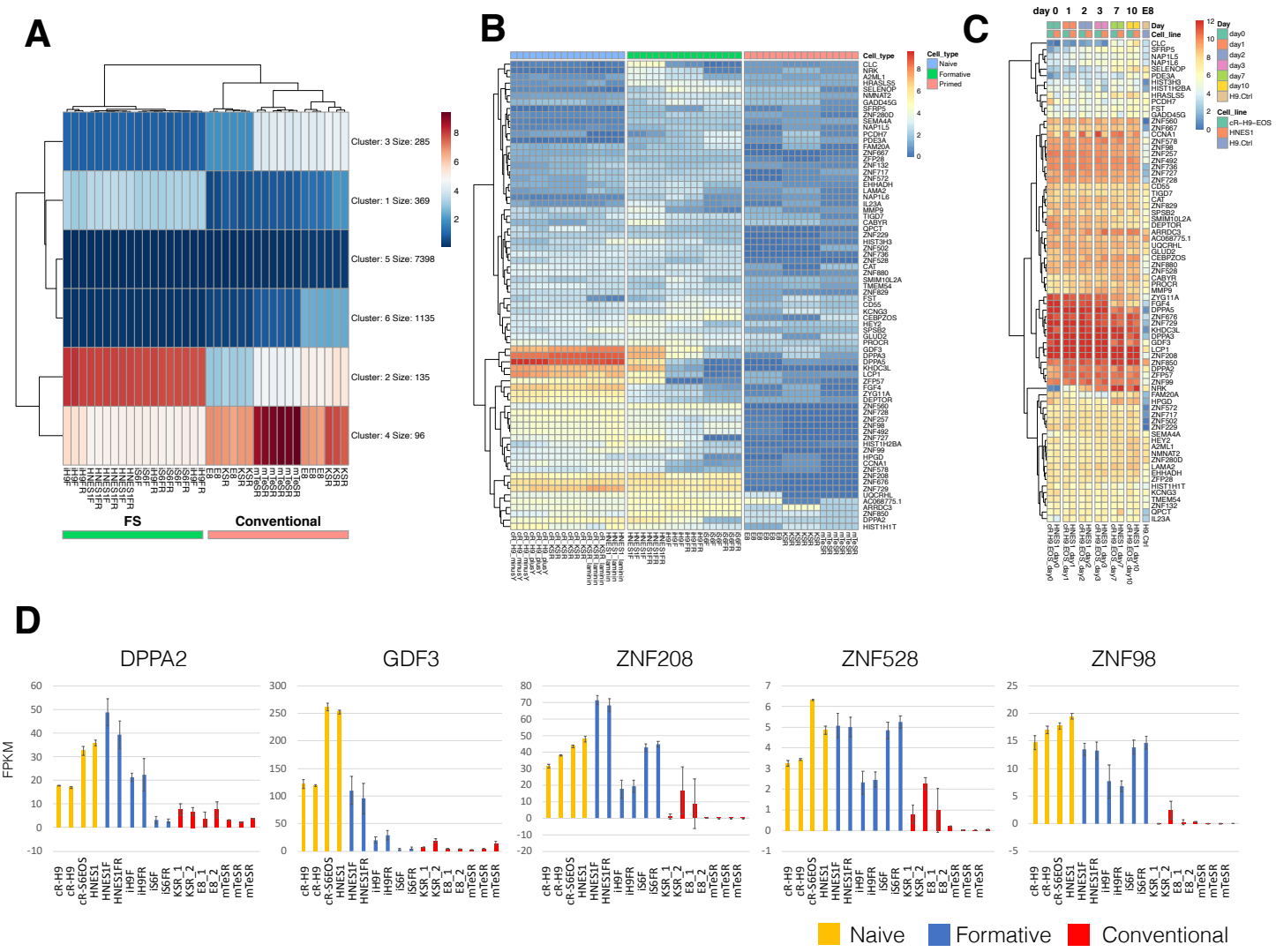

Supplemental Figure Legends

Figure S1. Derivation of stem cell lines from formative epiblast, Related to Figure 1
(A) Bright field image of E5.5 epiblast derived AFX and $A_{hi}X$ cultures. Scale bars, 200μm. (B) Gene expression analysis after FGF withdrawal. Three AFX cell lines (6, 27 and 33) were passaged without FGF and analysed by RT-qPCR. Error bars are S.D. from technical triplicates. (C) Immunostained images of early lineage marker expression in AFX and $A_{hi}X$ cells. Scale bars, 100μm. (D) Summary of derivation efficiency from E5.5 epiblasts in different concentrations of activin A. (E) RT-qPCR analysis of RAR inhibitor treated cells. $A_{lo}XR$ samples established in $A_{lo}X$ and transferred to $A_{lo}XR$ are in orange and a line derived in $A_{lo}XR$ in pink. Error bars, S.D. from technical triplicates. (F) Derivation efficiency in the absence of presence of RAR inhibitor. (G) Percentages of diploid cells for 4 FS cell lines. (H) Maximum projection of Z-stack slices of *Xist* RNA FISH images (red) in female FS cells. Nuclei were stained with DAPI (blue). Scale bar, 10μm. (I) Gene expression analysis by RT-qPCR during ES cell to FS cell conversion. Gene expression is relative to beta-actin. Error bars are S.D. from two technical replicates. (J) Flow cytometry analysis of day 4 PGCLC induction from $A_{lo}X$ FS cells. (K) Analysis of day 4 PGCLC induction from AFX EpiSCs. (L) Analysis of day 4 PGCLC induction from AFX EpiSCs adapted to culture in $A_{lo}XR$. (M) $A_{lo}XR$ cells sorted for SSEA1 and CD61 co-expression on day 6 of PGCLC induction (left) and subject to RT-qPCR analysis (right). Relative expression level to 2iL ES cells (=1) normalized to Tbp. Error bars represent S.D. from technical triplicates. (N) Immunostaining of $A_{lo}X$ cell-derived PGCLC. Scale bars, 50μm.

Figure S2. Lineage potency of FS cells and responsiveness to differentiation cues, Related to Figure 2
(A) Flow cytometry profiles of $Flk1^{+}Ecad^{-}$ mesodermal fraction of differentiated FS cells and EpiSCs at day 1 and day 2. (B) $Cxcr4^{+}Ecad^{+}$ endoderm fraction at day 3. Two experiments are shown. (C) RT-qPCR analysis after activin A and CH treatment for 3 days. AFX EpiSC samples at day 3 were set as 1, normalisation to 36B4 (Rplp0). Error bars represent SD from technical triplicates. n.d. not detected. (D) RT-qPCR analysis of T and Foxa2 expression 24 hours after indicated doses of Fgf2 were added into $A_{lo}XR$ culture. Error bars represent S.D. from technical duplicates.

Figure S3. Blastocyst chimaera contribution by FS cells and formative epiblast, Related to Figure 3
(A) Left, low contribution E9.5 chimaera produced from mKO2-labelled NBRA3.2 FS cells. Right, yolk sac contribution in one of the chimaeras in Fig. 3A. Scale bars, 500μm. (B) E9.5 chimaeras from GFP-labelled 5a6 FS cells. Contributions were widespread (left) or localised (right). Scale bars, 500μm. (C) E9.5 chimaeras from GFP-labelled 5ar1 FS cells. Scale bars, 500μm. (D) Sagittal section of embryo from C, left panel, with widespread contribution of GFP positive cells. Scale bar, 200μm. (E) Summary of FS cell chimaeras examined at E9.5. *Not all yolk sacs from chimaeric embryos were examined. (F) E12.5 chimaeric gonads generated from mKO2-labelled FS cells. Scale bars, 500μm. (G) Section of gonad from (F) stained with anti-Oct4 and anti-Mvh antibodies. Nuclei were stained with DAPI. (H-J). E9.5 chimaeras with contribution from E5.5 and E6.0 donor epiblast. Contributions were detected in the embryo proper and yolk sac (H), amnion (arrowhead) (I), yolk sac (J). Scale bars, 1mm. (K) Yolk sac section showing membrane-tdTomato positive cells in the inner layer of extraembryonic mesoderm. Nuclei were stained with DAPI (blue). Scale bar, 100μm. Magnified image from boxed region is shown as (K'). (L) Summary of post-implantation epiblast chimaeras.

Figure S4. Whole transcriptome analysis and nodal/activin pathway activity, Related to Figure 4

(A) Heatmap for top 50 differentially expressed genes (DEG) between FS cells and EpiSCs (AF). GO terms are shown (Benjamini value<0.05) for analysis of 200 DEG. (B) Heatmap for top 50 DEG between FS cells and EpiSCs (AFX). GO term analysis as in A (Benjamini value<0.05). (C) Example embryo gene expression profiles of FS cell enriched genes identified in Fig. 4B. E5.5 epiblast cells are highlighted by the dashed circle. (D) Heatmap of expression of Fgfs and Fgfrs. (E) Heatmap of Nodal pathway gene expression. (F) Heatmap of expression of Wnts and Fzd receptors. Colour scale in (D-F) is log2(normalised counts +1) from RNA-seq. (G) Cell morphologies after two days in indicated culture conditions: A_{lo}XR; 1μM A83-01 in A_{lo}XR; 5μM SB505124 in A_{lo}XR; without activin A in 2μM XAV939 and 1μM BMS493. Scale bars,100μm.

Figure S5. Chromatin landscape analysis, Related to Figure 5

(A) GO term enrichment for genes proximal to phase specific ATAC-seq sites. Bars in blue have a significant Benjamini value<0.05. (B) Enumeration of bivalent domains in each cell type. (C) Genome browser screenshots of differential histone modifications. Lower three examples show formative specific bivalency. (D) Methylation at ATAC peaks in EpiLCs and EpiSCs (original data from Zylicz et al., 2015). (E) Related to Fig. 5G. GO term analysis performed against significantly expressed genes in EpiSCs or FS cells. Bars in blue have a significant Benjamini value<0.05. (F) Transcription factor binding motifs and P-values enriched in phase specific ATAC sites.

Figure S6. Differential requirements for *Etv4/5* and *Otx2*, Related to Figure 6

(A) Schematic of ES cell differentiation to FS cells or EpiSCs and morphologies of *Etv4/5*dKO cells at day 2, P1 and P2. (B) Bright field image of contracting *Etv4/5*dKO differentiated cells. (C) Immunostaining of *Etv4/5*dKO FS cell EB outgrowth. Neuroectoderm stained with Sox1 (red) and Tuj1 (Blue), mesoderm with Gata4 (Green) and cTnT (blue), and endoderm with Ecadherin (red) and Foxa2 (Blue). DAPI stainings were shown in white. (D) Flow cytometry plot of endoderm differentiated *Etv4/5*dKO FS cells. (E) Immunostaining for Oct3/4 (green), Sox1 (red) and Tuj1 (Blue) after neural differentiation of *Etv4/5*dKO FS cells. (F) PGCLC induction from *Etv4/5*dKO FS cells analysed by flow cytometry for SSEA1-660 and CD61-PE and by immunostaining for Blimp1 (green), Stella (red) and Oct4 (blue). (G) Immunostaining of *Etv4/5*dKO FS cells in A_{lo}XR and after transfer to EpiSC culture (AFX) for three days. (H) *Otx2* KO cells passaged in A_{lo}XR with or without BMP. (I) Bright field image of *Otx2* KO FS cells re-plated in 2iL. Scale bars in (A), (B), (F), (H), (I) 100μm, (C) 250μm and (E), (G) 75μm.

Figure S7. Human FS-like cells established from naïve ES cells and embryos, related to Figure 7

(A) K-mean clustering of differential gene expression between human FS-like cells and conventional PSCs. (B) Gene expression heatmap for cluster 1 protein coding genes. (C) Expression heatmap of cluster 1 protein coding genes during naïve cell capacitation (data from Rostovskaya et al 2019). (D) Related to Figure 7I, FPKM values for additional selected naïve-formative specific genes. (E) Bar charts of differentially expressed TE families between formative and conventional hPSCs. (F) G-banded chromosomes from three independent human embryo derived FS-like cell lines.